University of Silesia

Department of Mathematics, Physics and Chemistry

Institute of Physics

Wojciech Gwizdała

The dynamics of *n*CB liquid crystals in confined space – computer simulation

The doctoral thesis carried out under the direction of

prof. dr hab. Zygmunt Gburski

in

Division of Computational Physics and Electronics

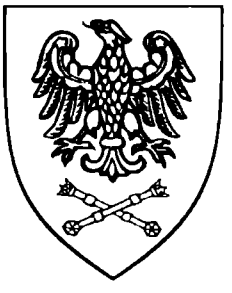

Katowice 2013

This thesis is dedicated to my wife Elżbieta and to our children.

I would like to thank my supervisor
prof. dr hab. Zygmunt Gburski
and other team members
for their support and valuable comments.

CONTENTS

INTRODUCTION

This thesis treats the physical properties of nematic liquid crystals placed in an unusual environment which includes some of the carbon allotropes like graphite, graphene and carbon nanotube. Despite the fact that liquid crystals are known and used in industry for many years, one can still see new papers coming from various research centers around the world. I performed series of computer experiments to explore new structural and dynamic properties of the chemical compound 4-n-pentyl-4'-cyanobiphenyl (5CB). All physical systems were modeled and numerical calculations performed using the computer simulation method. The work consists of two main parts. Its primary aim is to investigate the physical properties of small clusters of mesogen molecules 5CB located near the aforementioned carbon nanostructures. In the first part, which consists of three chapters, one can find essential knowledge about the examined compounds and an introduction to computer simulation techniques (Monte Carlo and molecular dynamics). The second part of this work (chapter 4 and 5) is based on my own research, some of them have been already published in international scientific journals. The last chapter of this dissertation is the analysis and discussion of results obtained from computer simulations of 5CB mesogens:

- located on the carbon nanostructure surface,
- confined inside carbon nanotube and between graphite or graphene walls.

The motivation to undertake such research topic is the urgent need to gain the detailed knowledge about molecular dynamics of mesogenes in such specific, confined spaces. Particularly, in a perspective of the presumed applications in a new generation of the future optical devices.

1

LIQUID CRYSTALS: DEFINITION, MAIN TYPES AND BASIC PROPERTIES

1.1 Definition of liquid crystals and history note

It is well known that matter can exist in four states: solid, liquid, gas and plasma. However, there are also some mespohases that exhibit properties typical for several other physical states [1]. The molecules in solids are constrained to occupy only certain positions, i.e. they have positional order. Furthermore, the molecules in these specific positions are also constrained in the way that they orient themselves with respect to each other, i.e. they have orientational order [2]. The solid may be either crystalline or amorphous. The molecules in liquids move and orient randomly, i.e. they lose positional and orientational order. The molecules in gases also move and orient randomly. The gas and the liquid states are very similar with certain differences: while in the liquid state the molecules keep an average distance to each other, in the gas state the average intermolecular distance is determined by the size of the container and the number of molecules. The flow is the most important property which differentiates solids and liquids. The liquids flow and adopt the shape of container, whereas solids do not flow and tend to retain their shape.

In the year 1888 an Austrian Botanist Reinitzer observed unusual sequence of phase transition. He observed two melting points while investigating some esters of cholesterol. At 145,5°C cholesteryl benzoate melted from a solid to a cloudy liquid and at 178,5 °C it turned into a clear liquid [*2*]. In particular, certain organic materials do not show a single transition from solid to liquid, but rather a cascade of transitions involving quite new phases. The mechanical and symmetry properties of these phases are intermediate between those of a liquid and those of a crystal. For this reason, they have often been called liquid crystals [1]. The molecules in liquid crystals move randomly like those in a liquid, i.e. they have no positional order, but they have some orientational order. A substance is isotropic when its physical properties are the same in all directions; like water at room temperature. Liquid crystals are anisotropic substances [3] because they exhibit different physical properties in different directions.

Although liquid crystals were discovered as an interesting phenomenon at the end of

the 19th century, it took over 30 years of research to establish their true identity. Georges Friedel in the 1920 was responsible for recognising that liquid crystals are indeed a new state of matter that is intermediate in structure and molecular organisation between the amorphous liquid state and solid crystalline state [3].

To understand better the significance of these new states of matters, it may be useful to recall first the distinction between a crystal and a liquid. The components of crystal (molecules, or groups of molecules) are regularly stacked. The mass centres of the various groups are placed in a three-dimensional periodic lattice. The centres of mass are not ordered in this sense in the liquid. These two states of matter differ most obviously by their mechanical properties; a liquid flows easily. A crystal is defined by the fact that, if a permitive pattern (or basis) is located at point x_0, the probability of finding an equivalent pattern at the point $x = x_0 + n_1a_1 + n_2a_2 + n_3a_3$ (n_i = integer; $i \notin \{1,2,3\}$ and $\{a_i\}$ basis vectors) stays finite when $|x - x_0| \rightarrow \infty$. As a result, its X-ray diffraction pattern shows sharp Brag reflections characteristic of the lattice. An isotropic liquid may be defined in a similar way. One can say that, if one has been able to locate a molecule or some pattern at a given point x_0, there is just no way to express the probability of finding a similar one at the point x far from x_0, except through the average particle density [1].

We are now able to give the definition of liquid crystals. These are systems in which a liquid-like order exists at least in one direction of space and in which some degree of anisotropy is present (a better definition of „some degree of anisotropy" is: density-density correlation function does not depend solely on modulus $|x - x'|$ but also on the orientation of $x - x'$ with respect to macroscopically defined axes) [1].

1.2 General types and liquid crystal phases

Considering the geometrical structure of the mesogenic molecules, the liquid crystals can be grouped into several types. The mesophases formed from disc-like molecules (one molecular axis is much shorter than the other two) are referred to as „discotics" (Fig. 1.1a). The liquid crystals derived from the rod-shaped molecules (one axis is much longer than the other two) are called „calamitics" (shown in Fig. 1.1b). This class of materials is well known and extremely useful for the practical aplications [2]. Transitions to the mesphases may be brought about in two different ways; one by ordinary thermal processes and the other by influence of solvents. The liquid crystals obtained by the first method are called

„thermotropics" whereas those obtained by the second one are „lyotropics". This work focuses on dynamical and structural properties of the „thermotropic" rod-like mesogens.

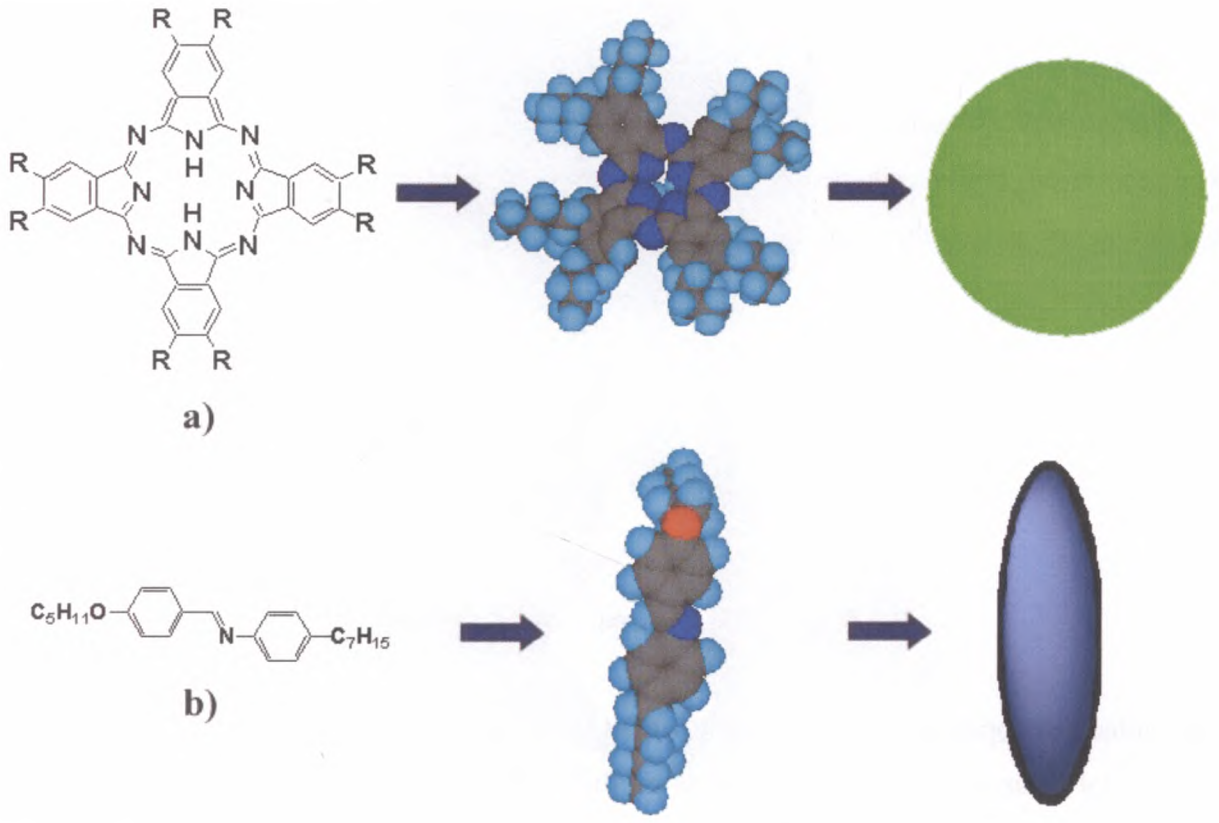

Fig. 1.1 a) Phthalocyanine and disc-shape; **b)** 4-*n*-heptyl-*N*-(4-*n*-pentyloxy) benzylideneand rod-shape

As far as we know there are several liquid crystalline phases. The simplest one could imagine is a phase in which the molecules are oriented among a common direction in space, and the positions of the molecules are totally random [4]. In other words, molecules have no positional order but they self-align to have long-range directional order with their long axes roughly parallel. Schematic picture of this phase is shown in Fig. 1.2.

Fig. 1.2 Nematic phase represented schematically

The molecules appear to be able to rotate about their long axes and also there seems to be no preferential arrangement of the two ends of the molecules if they differ. This phase is an oriented or anisotropic liquid. Such liquids are frequently observed in nature and are called nematic liquid crystals. Many compounds are known to form nematic mesophase. A few typical examples are sketched in Fig. 1.3.

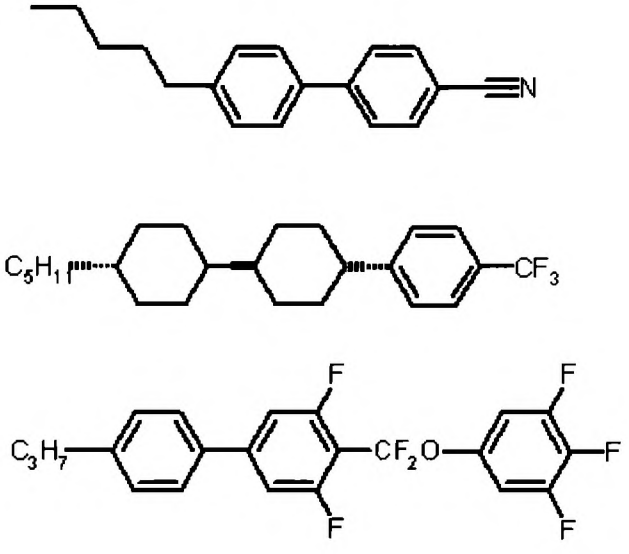

Fig. 1.3 Nematic molecules; this is a rigid rod of length ~ 20 Å and width ~ 5 Å

The cholesteric phase looks like the nematic phase in having long-range orientation order and no long-range order in positions of the centres of mass of molecules (Fig. 1.4). This distortion was first observed in liquid crystals which contain cholesterol, so, for historical reasons, this structure, which is a unique phase, is called the cholesteric liquid crystalline phase. There are many liquid crystals which exhibit a cholesteric phase yet but have no connection to cholesterol. For this reason, a much better name to use is chiral nematic or twisted nematic. Locally, a cholesteric seems to be like a nematic. When the structure is studied over large enough distances it appears that the cholesteric phase appears to have a structure different from the nematic phase [4].

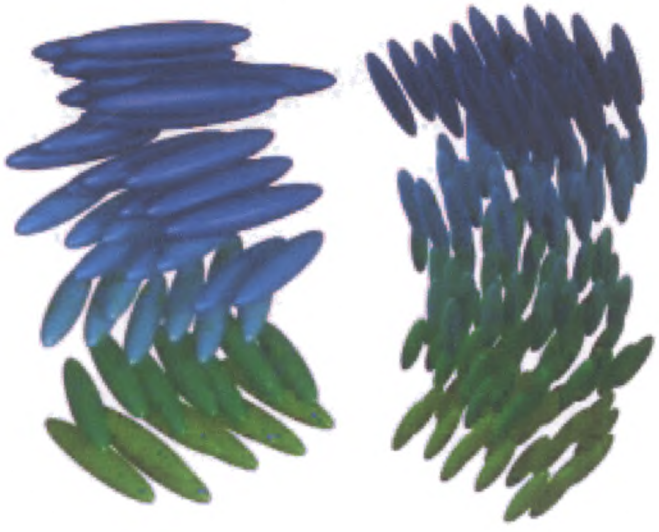

Fig. 1.4 Cholesteric phase

Suppose now that a phase forms in which the long-range orientational order is maintained and long-range periodicity is found, not in three dimensions as in a crystal, but only in one dimension. This can be thought of as a stack of two-dimensional liquid surfaces. The spacing between these liquid surfaces extends over very long distances resulting in a phase with long-range orientational order and long-range positional order in one dimension. This type of liquid crystalline phase exists also in nature and is known as a smectic liquid crystal. The molecules are arranged in layers and show some correlations in their positions in addition to the orientational ordering. Different types of smectics have been recognized and classified. In smectic A phase the molecules are aligned perpendicular to the layers, with no long-range crystalline order within a layer (see Fig. 1.5). The layers can slide freely over one another. In turn, the preferred axis is not perpendicular to the layers in the smectic C phase, so that the phase has biaxial symmetry. There is hexagonal crystalline order within the layers visible in smectic B phase.

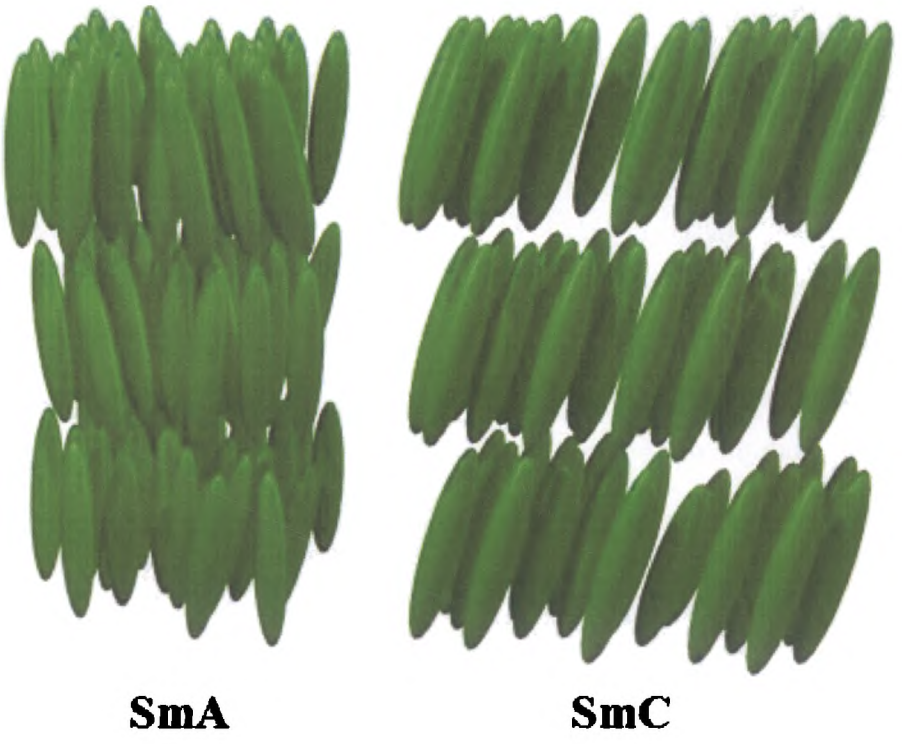

Fig. 1.5 Smectic A representation (left); Smectic C representation (right)

The other most complex phase would be a phase that has long-range orientational order and long-range positional order in two dimensions. Such a phase can be described as a two-dimensional array of liquid tubes. Such phases are also observed and are called columnar phases.

All listed and discussed phases (nematic, smectic and columnar) are the only known liquid crystalline phases. However, slight variations in these basic phases occur and lead to hyphenated names for some existing phases. The type of phase observed depends very strongly on the structure of the constituent molecules or, in some situations, the agregates that consitute the phase. Nematics and smectics are most often observed when elongated or rod-like molecules order. Columnar phase are often observed when disc-like molecules order [4].

1.3 Physical properties of liquid crystals

Liquid crystalline materials are anisotropic because they are composed of anisotropic molecules. Some of their physical properties depend on the direction along which they are measured. Such properties are known as tensor properties. A comfortable way of categorizing

tensor properties is through their behaviour on changing the orientation of coordinate system. A scalar or zero rank tensor is independent of direction. Good examples are density, volume, energy or any orientationally averaged property such as the mean polarizabilty or mean electric permitivity (dielectric constant). The orientation dependence of a vector property such as dipole moment μ can be explain by considering how the components of the dipole moment change as the coordinate system axis are rotated [6].

The liquid crystalline materials exhibit anisotropy in many of their physical properties. Due to these anisotropies and their resulting interactions with the surrounding environments a number of phenomena are found in a liquid crystalline phase which are absent in the isotropic liquid phase. In the following, a brief discussion is given on some of these properties.

Liquid crystals sensitivity to an electric field is well known. It allows their application in displays and other optical device technology. The most physical parameters of materials are based on the electrooptical measurements. The optical anisotropy is an essential physical property for the optimization of liquid crystal compounds for application in liquid crystal devices. The velocity of light wave propagation in the medium is no longer uniform but is dependent upon the direction and polarization of the light waves transversing the material; thus the material is found to possess different refractive indices in different directions. Aligned liquid crystals allow to control the polarization of light which has resulted in the use of liquid crystals in displays [2]. The ordinary refractive index n_0 can be observed with a light wave where the electric vector oscillates perpendicular to the optic axis. The extraordinary refractive index n_e is observed for a linearly polarized light wave where the electric vector is vibrating parallel to the optic axis. The optic axis of the uniaxial mesophases is represented by the director. The optical anisotropy, or birefringence is wavelenght and temperature dependent and defined by the equation

$$\Delta n = n_e - n_0 = n_{\parallel} - n_{\perp}, \qquad (1.1)$$

where $n_{\parallel}$ and $n_{\perp}$ are the components parallel and perpendicular to the director, respectively [2].

Polarizability:

Electric field can polarize all atoms and molecules. The polarization (induced dipole of a unit volume) $\vec{P} = \alpha \vec{E}$ where α is molecular polarizability and $\vec{E}$ is intensity of electric field. For spherically symmetry objects – atoms or molecules (like C_{60} fullerenes) the

polarizablity is a scalar quantity (tensor of zero rank) and $\vec{P}\|\vec{E}$. In general case of lath-like molecules, α_{ij} is a second rank tensor (consisted of 9 components) and $\vec{P}_j=\alpha_{ij}\vec{E}_i$ by a proper choice of the reference frame the tensor can be diagonalized

$$\alpha_{ij}=\begin{bmatrix}\alpha_{xx} & 0 & 0\\ 0 & \alpha_{yy} & 0\\ 0 & 0 & \alpha_{zz}\end{bmatrix} \tag{1.2}$$

and components α_{xx}, α_{yy} and α_{zz} repersent three principal molecular polarizabilities. For molecules which have cylindrical symmetry (rods or disks) with the symmetry axis z, only two different components remain $\alpha_{xx} = \alpha_{yy} = \alpha_{\perp}$ and $\alpha_{zz} = \alpha_{\|}$.

Permanent dipole moments:

If a molecule have an inversion centre it is non-polar and its dipole moment (a vector, a tensor of rank 1) $\vec{p}_e=0$. Dipole moment is finite in less symmetric case. This observable is measured in units Debye and in the Gauss system 1 $D = 10^{-18}\ CGSQ \cdot cm$ ($3{,}3 \cdot 10^{-30}\ C \cdot m$ in *SI* system). In other words, 1 D corresponds to one electron positive and one electron negative charge separated by a distance of $\approx$ 0.2 Å. For complex molecule $\vec{p}_e$ can be estimated as a vector sum of the moments of all intramolecular chemical bonds, $\vec{p}_e=\sum \vec{p}_i$. Classical example is shown in (Fig. 1.6). A molecule of 5CB (4-n-pentyl-4'-cyanobiphenyl), strongly investigated in this work, has a longitudinal electric dipole moment about 3D due to a triple -C≡N bond.

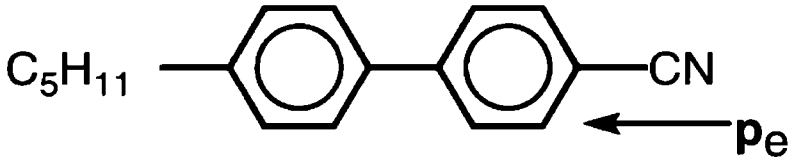

Fig. 1.6 The mesogen molecule 5CB

The vector of a permanent dipole moment and polarizability tensor is used to describe the linear (in field) electrical and optical properties. The nonlinear properties are described by tensors of higher ranks (this depends of the number of fields included).

Magnetic moments:

A magnetic field induces magnetic moments in a molecule and it is given by relation: $p_{mi} = m_{ik} \cdot H_k$, where m_{ik} is the diamagnetic suscebtibility tensor. It has the same structure as

the tensor of molecular polarizability with three or two different principal components. Some molecules possess permanent magnetic moments. For example, the moments originate from unpaired electron spins in the inner shells of such metal atoms as M = Ni, Co, Fe, etc. in metal-mesogenic compounds. Other case depend on free radicals with permanent magnetic moments of such molecular groups as –NO, in which unpaired electron spins are placed on oxygen atoms. Stability of such radicals is provided by sterical screening of a reaction centre from the surrounding medium by bulky chemical groups (like methyl one). Such a radical can be a fragment of a longitudinal mesogenic molecule. It is important that the field orientation of spin moments is almost decoupled from the molecular skeleton motion (in contrast to electric moments of molecular groups). It should be noted that the simultaneous orientation of spins and molecular skeletons by a magnetic field takes place only if the so-called spin-orbital interaction is significant [7].

1.4 Molecular ordering

In the crystalline (solid) state, molecules usually have near-perfect orientational order. In the mesophase this degree of order is partially but not completely lost, as the molecules show highly dynamic behavior and only on average point in the same direction. In fact, the molecules spend little more time pointing along a common orientation axis than they do in any other direction but they do so sufficiently long enough for there to be orientational order. This preferred direction is called the director (Fig. 1.7). The most common liquid crystalline phase (nematic) has a lower symmetry than the high-temperature isotropic liquid so it means the nematic phase is „more ordered". The degree of order is described by the order parameter (S), which is a measure for the average angle 0 between the director and the long axes of the mesogens. It is essential to define an order parameter that is non-zero in the nematic phase but that vanishes in the isotropic phase. For an isotropic sample, $S = 0$, whereas for a perfectly aligned crystal $S = 1$. For a typical liquid crystal, S is between 0.3 to 0.8, and this value generally decreases due to higher mobility and disorder as the temperature is raised (thermotropic mesogens). In some physical ensembles an adequate choice of the order parameter is obvious. For instance, in a ferromagnet, the magnetization M is the order parameter and in a such case this is a vector with the three independent components M_Φ. In a nematic phase the choice is less trivial and we shall have to proceed in successive steps [1].

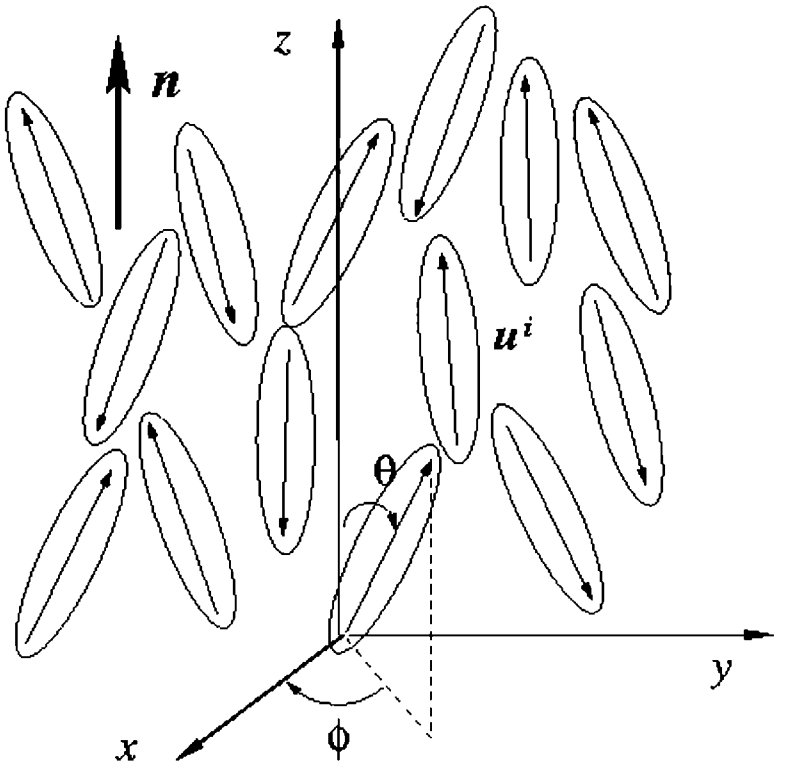

Fig. 1.7 A unit vector u^i along the axis of ith molecule describes its orientation. The director n shows the average alignment

If the laboratory Z axis is taken parallel to the director and if the mesophase is uniaxial around the director then rotating the sample about Z should leave all observable properties unchanged. This means that the probability for a molecule to have an orientation (Φ, θ) is the same whatever the angle α [8]. More precisely

$$P(\phi,\theta)=\frac{P(\theta)}{2\pi} \quad . \tag{1.3}$$

Another experimental finding for nematics is that nothing changes on turning the aligned sample upside down. It is described by formula

$$P(\theta)=P(\pi-\theta) \quad . \tag{1.4}$$

This is quite reasonable for considering of the molecules of interest as spherocylinders or other cylindrically symmetric objects in which head and tail are not distinguishable. However, most mesogens are not like this and for instance have dipole moments like p-n alkyl p'-cyano biphenyls (*n*CB). In practice the symmetry eq. 1.4 means that the molecular arrangement will be such as to have on average no overall polarization (no ferroelectricity) as we show schematically in Fig. 1.8. It is impossible to give fundamental argument that forbids uniaxial ferroelectric fluids and indeed these have been predicted by theory and simulations [9], although not yet experimentally found. Notice that the same notation for $P(\theta)$ and $P(\cos\theta)$ has

been used, that we assume to be renormalized to 1.

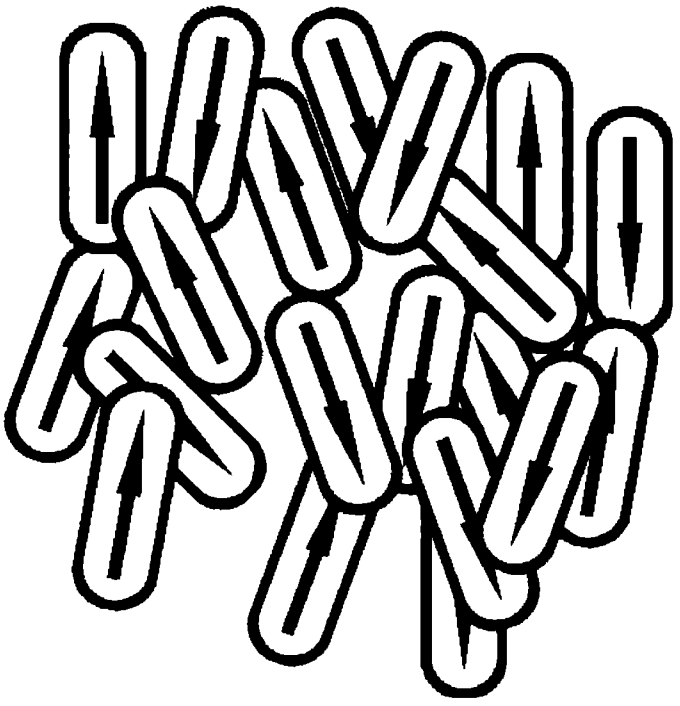

Fig. 1.8 Schematic molecular organization for a system of polar molecules without overall polarization

In a real experiment it could be extremely difficult to get this kind of complete information on the orientational distribution. A useful approach is, however, that of expanding $P(\theta)$ and approximating it in terms of a set of quantities that could be obtain from experiment. A set of functions (orthogonal) is necessary when integrated over $d\theta \sin\theta$ Such a set of functions is that of Legendre polynomials $P_L(\cos\theta)$, for which following formula is given

$$\int_0^{\pi} d\theta \sin\theta P_L(\cos\theta) P_N(\cos\theta) = \frac{2}{2L+1}\delta_{LN} \quad . \tag{1.5}$$

The explicit form of these Legendre polynomials is not very complex [10] and the first few terms are

$$P_0(\cos\theta) = 1 \quad , \tag{1.6}$$

$$P_1(\cos\theta) = \cos\theta \quad , \tag{1.7}$$

$$P_2(\cos\theta) = \frac{3}{2}\cos^2\theta - \frac{1}{2} \quad , \tag{1.8}$$

$$P_3(\cos\theta) = \frac{5}{2}\cos^3\theta - \frac{3}{2}\cos\theta \quad , \tag{1.9}$$

$$P_4(\cos\theta) = \frac{35}{8}\cos^4\theta - \frac{30}{8}\cos^2\theta + \frac{3}{8} \quad . \tag{1.10}$$

It is worth noting that $P_L(\cos\theta)$ is an even function of $\cos\theta$ if the rank L is even and an odd one if L is odd. Since $\cos(\Pi-\theta) = -\cos\theta$ this means that in writing even orientational distribution in terms of $P_L(\cos\theta)$ functions only even L terms need to be kept. Clearly the odd terms will be exhibit if $P(\theta)$ is not even, as for ferroelectric liquid crystalline phases. Limiting ourselves to the more common even (see eq. 1.4) case it can be give as

$$P(\theta)=\sum_{L=0}^{\infty}\frac{2L+1}{2}\langle P_L\rangle P_L(\cos\theta) \quad \text{, for } L = 0, 2, 4, \ldots \tag{1.11}$$

where the coefficients have been obtained exploiting the orthogonality of the basis set. The average values of $\langle P_L\rangle$:

$$\langle P_L\rangle=\frac{\int_0^{\pi} d\theta \sin\theta P_L(\cos\theta)P(\theta)}{\int_0^{\pi} d\theta \sin\theta P(\theta)} \tag{1.12}$$

represent set of orientational order parameters. The knowledge of the set of $\langle P_L\rangle$, which is infinite, would completely define the distribution. The next formula arises from eq. 1.11

$$P(\theta)=\frac{1}{2}+\frac{5}{2}\langle P_2\rangle P_2(\cos\theta)+\frac{9}{2}\langle P_4\rangle P_4(\cos\theta)+\ldots \quad . \tag{1.13}$$

The first term contains the second rank order parameter

$$\langle P_2\rangle=\frac{3}{2}\langle\cos^2\theta\rangle-\frac{1}{2} \quad . \tag{1.14}$$

It is really easy to see that $\langle P_2\rangle$ has the properties that are expected an order parameter to possess and that can be identified with the empirical parameter which was introduced by Tsvetkov [11]. For a system of perfectly aligned mesogenic molecules, where $\theta = \theta$ for every molecule, $\langle P_2\rangle = 1$. At the other extreme, for a completely disordered sample such as an ordinary isotropic fluid $\langle\cos^2\theta\rangle = 1/3$ and thus $\langle P_2\rangle = \theta$. In general case

$$-\frac{1}{2}\le\langle P_2\rangle\le 1 \tag{1.15}$$

because $\theta \le \cos^2\theta \le 1$. Transition from an ordered to a disordered system the order parameter jumps discontinuously to zero if the transition is of the first order type, like the nematic-isotropic one. It is worth to know that the same $\langle P_2\rangle$ can be compatible with different molecular organizations [12, 13].

2

FORMS OF CARBON: DIAMOND, NANOTUBES, GRAPHITE AND GRAPHENE

2.1 The chemistry of carbon atom

Carbon is essential to all known living systems, and without it life as we know it could not exist. Carbon atom is placed directly above silicon on the periodic table and therefore both have 4 valence electrons. These valence electrons give rise to $2s$, $2p_x$, $2p_y$, and $2p_z$ orbitals while the 2 inner shell electrons belong to a spherically symmetric $1s$ orbital that is tightly bound and has an energy far from the Fermi energy of carbon atom. Because of this reason, only the electrons in the $2s$ and $2p$ orbitals contribute to the solid-state properties of graphite. This extraordinary ability to hybridize sets carbon apart from other elements and allows carbon to form 0D, 1D, 2D, and 3D structures (Fig. 2.1) [14].

The applications of carbon and its compounds are extremely varied. It can form alloys with iron, of which the most common is carbon steel. Graphite is combined with clays to form the „lead" used in pencils. It is also used as a lubricant and a pigment, as a molding material in a glass manufacture, in electrodes for dry batteries, in brushes for electric motors and as a neutron moderator in nuclear reactors.

2.2 Carbon allotropes

Diamond:

The diamond is three dimensional form of carbon. It is $sp3$ bonded forming 4 covalent bonds with the neighboring carbon atoms into a face-centered cubic atomic structure which is shown (Fig. 2.1a). Because the carbon-carbon covalent bond is known as a one of the strongest in nature, diamond has a remarkably high Young's modulus and high thermal conductivity. Undoped (pure) diamond has no free electrons and is a wide band gap (~5.5 eV) insulator [15]. The exceptional physical properties and clever advertising such as "Diamonds are forever" contribute to its appeal as a sought after gem. It is possible to make beautiful

pieces of jewelry, only when carefully cut and polished. Crystals with smaller defects are used as reinforcement in tool bits which utilize its superior hardness for cutting applications. The high thermal conductivity of diamond makes it a potentially useful material for microelectronics where there is a problem with heat dissipation. However, diamond's scarcity makes this unappealing. To this end, scientists and engineers are focused on trying to grow large diamond wafers. One method to do this is chemical vapor deposition (CVD) where solid carbon is deposited from carbon containing gases such as methane or ethylene. By controlling the growth conditions, it is possible to produce high quality diamonds (without defects) of limited size. This technique is widely used to produce diamonds for jewelry and research is ongoing to scale the technology up to wafer size diamond growth. It is only with such large scale growth that diamond will make any technological impact beyond its current industrial uses in the machining industry.

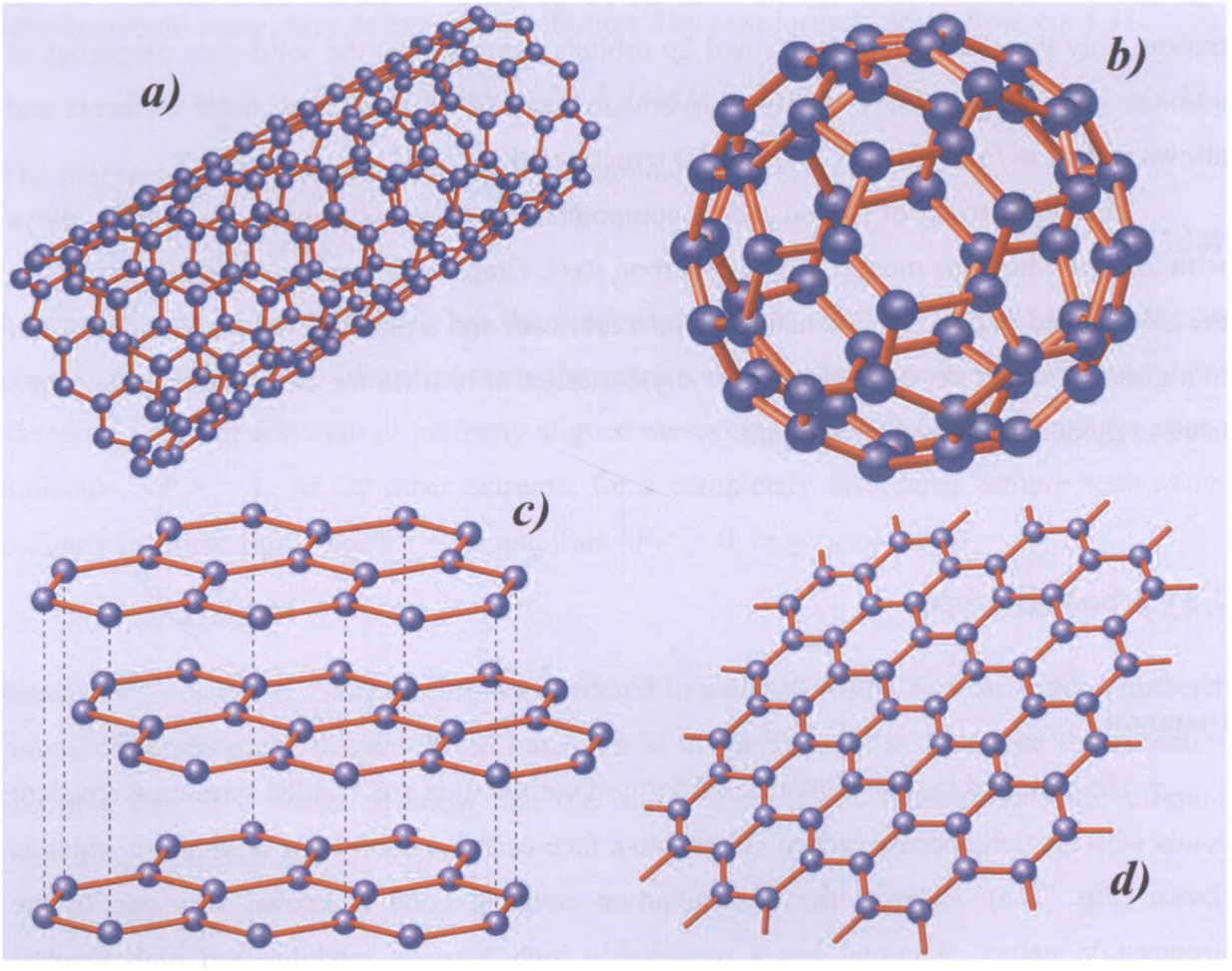

Fig. 2.1 a) Single walled carbon nanotube **b)** Buckminsterfullerene (C_{60}) **c)** Graphite lattice **d)** Graphene sheet

Fullerenes:

Carbon exists also in more exotic low dimensional forms known as the fullerenes which consist of the 0 dimensional C_{60} molecule (Fig. 2.1b) and its 1 dimensional derivative, carbon nanotubes. A single walled carbon nanotube (SWCNT) is a graphene sheet rolled into a cylindrical tube with a ~ 1 *nm* diameter (Fig. 2.1a). The first reported observation of carbon nanotubes was by Iijima in 1991 for multi-wall nanotubes (MWNT) [16]. Two years later, single walled carbon nanotubes were discovered experimentally by Iijima [17] at the NEC Research Laboratory in Japan and by Bethune [18] at the IBM Almaden Laboratory in California. These experimental discoveries and the theoretical works, which predicted many remarkable and interesting properties for carbon nanotubes, launched this field and propelled it forward. Carbon nanotubes can be both metals or semiconductors and have mechanical strength similar to diamond. These carbon allotropes attracted a lot of attention from the research community and dominated the scientific headlines during the 1990s and early 2000. This interest in carbon nanotubes was partly responsible for the search for planar two-dimensional planar carbon structures as a potentially important and interesting material for electrical and mechanical applications [19-21].

Graphite and Graphene:

Graphene and graphite are the two-dimensional sp2 hybridized forms of carbon, used in pencil lead. Graphite is a layered material formed by stacks of graphene planes separated by 0.335 *nm* and held together by weak van der Waals forces (Fig. 2.1c) [22]. This type of interaction between the sheets allows them to slide relatively easily across one another. This gives pencils their writing ability and graphite its lubricating properties, however the nature of this interaction between layers is not quite understood. It has been well known for decades that the presence of water reduces the frictional force considerably [23]. Another frictional effect seems to be important is the registry of the lattice between the layers. Mismatch in this registry is believed to give graphite the property of superlubricity where the frictional force is reduced distinctly [24]. Zheng [25] claims that mechanical experiments based on few layer graphene may help to elucidate some of these mechanisms clearly. A single 2D surface of graphene is a hexagonal structure with each atom forming 3 bonds with each of its nearest neighbours (Fig. 2.1d). These are the σ bonds oriented towards these neighbouring atoms and formed from 3 of the valence electrons. These covalent carbon-carbon bonds are nearly the same as the bonds holding diamond together giving graphene similar mechanical and thermal

properties as diamond. The fourth valence electron does not participate in covalent bonding at all. It is in the $2p_z$ state oriented perpendicular to the plane of graphite and forms a conducting π band. The unusual electronic properties of carbon nanotubes are a direct consequence of the peculiar band structure of graphene, a zero bandgap semiconductor with 2 linearly dispersing bands that touch at the corners of the first Brillouin zone [26]. Bulk graphite has been intensively investigated for decades [22] but until recently there were no experiments on graphene. This was due to the difficulty in separating single layers of graphene for study. In 2003, Novoselov and Geim succeeded in producing the first isolated graphene flakes [27].

3

COMPUTER SIMULATION: MOLECULAR DYNAMICS SIMULATIONS AND MONTE CARLO METHOD

3.1 Introduction to computer simulations

Before computer simulation appeared as a research technique, there was only one way to predict the properties of a molecular substance, namely by making use of a theory that provided an approximate description of that material. Such approximations are inevitable inaccurate because there are very few systems like for instance the ideal gas, the harmonic crystal, and a number of lattice models, such as the two-dimensional Ising model for ferromagnets for which the equilibrium properties can be computed exactly. Most properties of real materials were predicted on the basis of approximate theories (good examples are the van der Waals equation for dense gases, the Debye-Htickel theory for electrolytes, and the Boltzmann equation to describe the transport properties of dilute gases). Having information about the intermolecular interactions, these theories will provide us with an estimate of the properties of interest. Our knowledge of the intermolecular interactions of all but the simplest molecules is also quite limited. This leads to a problem if we want to test the validity of a particular theory by comparing to experiment. If we find that theory and experiment disagree, it may mean that our theory is wrong, or that estimate of the intermolecular interactions is incorrect, or both [28]. It is now over 60 years since the first computer simulation of a liquid was performed by Metropolis et al., at the Los Alamos National Laboratories in the United States [29]. MANIAC - the Los Alamo's computer was at that time one of the most powerful available; it is a measure of the recent rapid advance in computer technology that microcomputers of comparable power are now available to the general public at moderate cost [30]. The two main families of computer simulations are molecular dynamics (MD) and Monte Carlo (MC); additionally, there is a whole range of hybrid techniques which combine features from both.

Early models of liquids involved the physical manipulation and analysis of the packing of a large number of gelatine balls, representing the molecules; this resulted in a surprisingly

good three-dimensional picture of the structure of a liquid and later applications of the technique have been described. Even nowadays, there is some interest in the study of assemblies of metal ball bearings, kept in motion by mechanical vibration. However, the use of large numbers of objects to represent molecules can be very time-consuming, there are obvious limitations on the types of interactions between them, and the effects of gravity can never be eliminated. The natural extension of this approach is to use a mathematical model and to perform the analysis by computer [30].

From the outset, computers have been played a central role in scientific research, both in experiment and in theory. For the theoretician physicist, the computer has provided a new paradigm of understanding. Rather than attempting to obtain simplified closed-form expressions that describe behavior by resorting to approximation, the computers are now able to examine the original system directly. Despite the fact that there are no analytic formulas to summarize the results neatly, all aspects of the behaviour are open for inspection [31].

3.2 Atomic model and interaction potential

The most simple microscopic model for a substance capable of existing in any of the three most familiar states of matter – solid, liquid and gas – is based on spherical particles. They interact in one another; in the interest of brevity such particles will be reffered to as atoms. The interactions, at the simplest level, occur between pairs of atoms and are responsible for providing the two principal features of an interatomic force. A resistance to compression is the first one, hence the interaction repels at close range. The second is to bind the atoms together in the solid and liquid states, and for this the atoms must attract each other over a range of isolation. Potential functions, which exhibit these characteristics can adopt a variety of forms and actually provide useful models for real substances.

The most popular of these potentials, originally proposed for liquid argon, is the Lennard-Jones (LJ) potential V_{LJ} (Fig. 3.1), that depends on two parameters: length-scale parameter σ , and energy-scale parameter ε. The simplest form of $V_{LJ}(r)$ is given via formula:

$$V_{LJ}(r_{ij}) = 4\epsilon_{ij}\left[\left(\frac{\sigma_{ij}}{r_{ij}}\right)^{12} - \left(\frac{\sigma_{ij}}{r_{ij}}\right)^{6}\right] \tag{3.1}$$

for a pair of atoms i and j located at $\vec{r}_i$ and $\vec{r}_j$ respectively, $r_{ij} = |\vec{r}_i - \vec{r}_j|$, $r_{ij} < r_c$, and

zero otherwise. If r increases towards r_c (cutoff radius) the potential energy $V(r)$ drops to zero,

$$V(r)=\begin{cases} V_{LJ}(r), r \le r_c \\ 0, r > r_c \end{cases} . \tag{3.2}$$

Ignoring calculations of all interactions beyond r_c is the simplest method to truncate potential. This kind of numerical trick is often used in performing simulations of a systems with short-range interactions. The equations of motion imply from Newton's second law:

$$m_j \ddot{\vec{r}} = \vec{F}_i = \sum_{j=1,(j\neq i)}^{N_m} \vec{F}_{ij} , \tag{3.3}$$

where the sum is over all N_m interacting atoms, excluding i itself, and m is the atomic mass. These equations must be numerically integrated. Newton's third law shows that $F_{ji} = - F_{ij}$ so each atom pair needs to be examined only once. The amount of interactions is proportional to N_m^2 , so that for models in which cutoff distance r_c is small compared with the size of the container it would be a good idea to determine those atom pairs for which $r_{ij} \le r_c$ and use this information to reduce the computational effort [31].

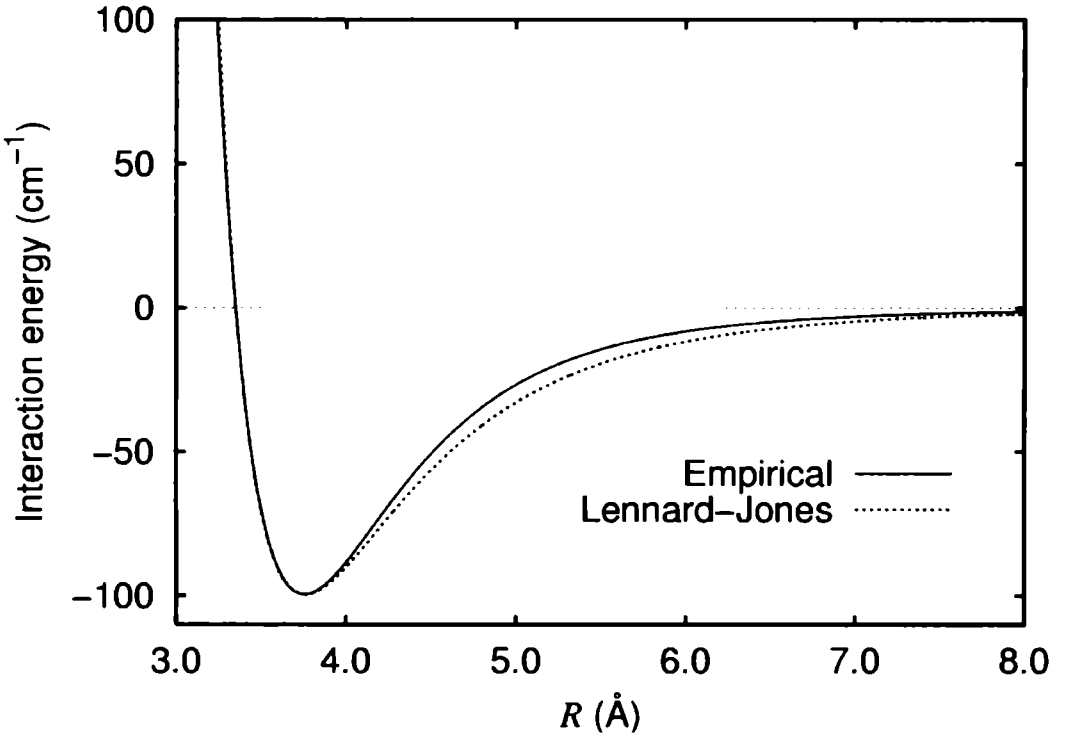

Fig. 3.1 Lennard-Jones potential for the argon dimer

3.3 Molecular dynamics

Molecular dynamics is a method for computing the equilibrium and transport properties of a classical many-body ensemble: transport coefficients, time-dependent responses to perturbations, rheological properties and spectra. In this context, „classical" means that the nuclear motion of the constituent particles obeys the laws of classical mechanics. This is a good approximation for a wide range of materials. Only for the translational or rotational motion of light atoms or molecules (He, H_2, D_2) or vibrational motion with a frequency ν, such that $h\nu > k_B T$ quantum effects are important [28].

Computer simulations based on MD are in many respects very similar to real experiments. When we want to perform a real experiment, we proceed as follows. We have to prepare a sample of the material that we wish to study. We connect our sample to a measuring instrument (a thermometer, manometer, or viscosimeter), and we start to measure the property of interest during a certain time interval. If our measurements are subject to statistical noise, then the longer we average, the more accurate our measurement becomes. In a molecular dynamics simulation, we need to do exactly the same steps. In the first instance, we select a model system consisting of N particles and we solve Newton's equations of motion for this system until the averages of the system no longer change with time (we equilibrate the system). After this, we perform the actual measurement. Actually, some of the most common mistakes that can be made when performing a computer simulation are very similar to the mistakes that can be made in real experiments. For example: the sample is not prepared correctly, the measurement is too short, the system undergoes an irreversible change during the experiment, or we do not measure what we think [28].

3.3.1 Simple molecular dynamics algorithm

The good introduction to molecular dynamics is to consider a quite simple program. The program we consider is kept as simple as possible to illustrate a number of important features of molecular dynamics simulations. The algorithm consists of several essential steps:

1. We initialize the system (we select initial positions and velocities).
2. We compute the forces on all particles.

3. We integrate Newton's equations of motion. This step and the previous one make up the core of the simulation. They are repeated until we have computed the time evolution of the system for the desired length of time.
4. After completion of the central loop, we compute and print the averages of measured quantities, and stop.

The pseudo-algorithm described above would carry out a molecular dynamics simulation for a simple atomic system. The different procedures in the program are discussed later in more detail. The programming task could be more clear and better understood when we look at algorithm scheme attached below.

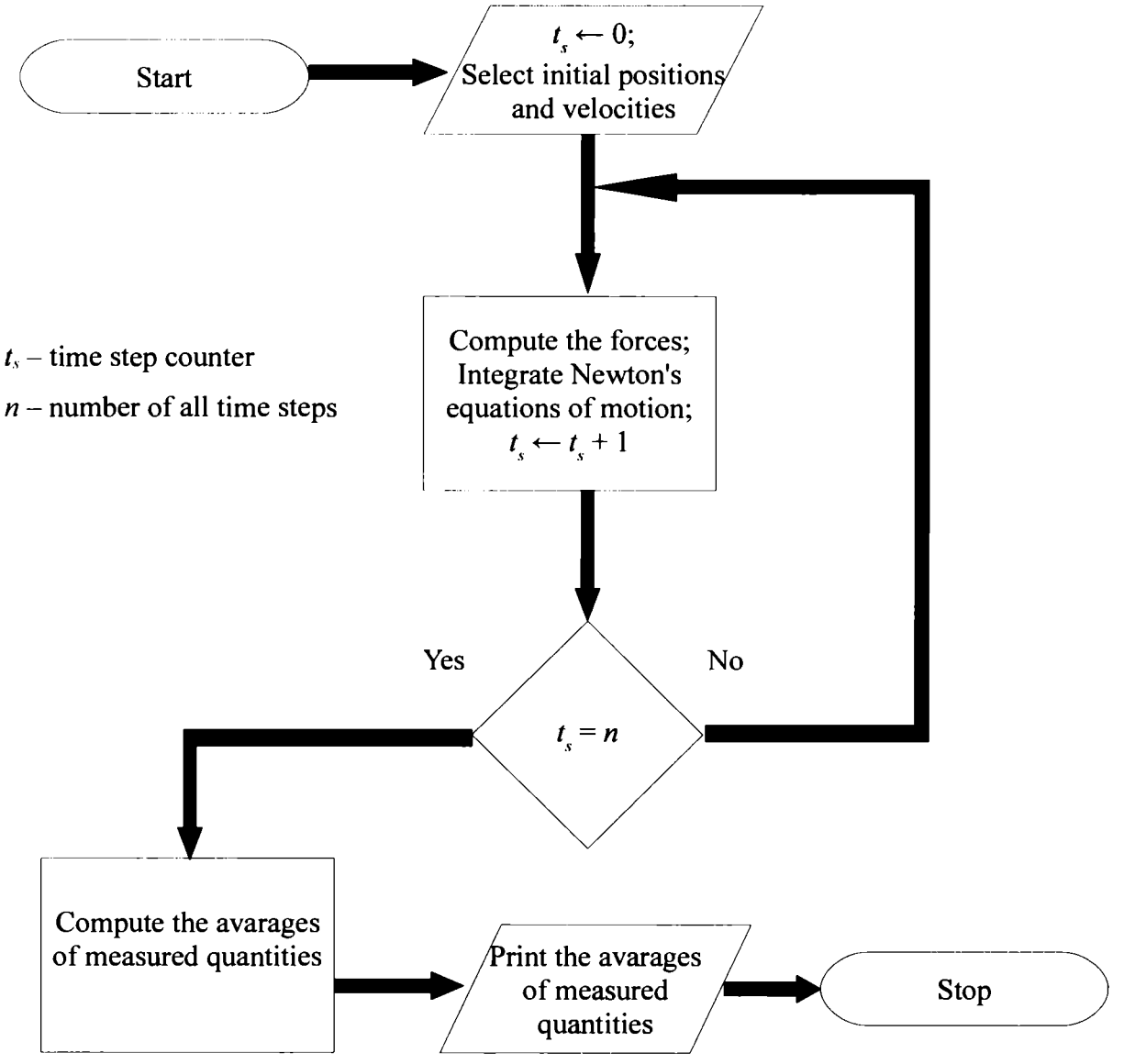

Initialization is the first step in MD algorithm. To start the simulation, we should assign initial positions and velocities to all particles in the system. The particle positions should be chosen compatible with the structure that we are aiming to simulate. In any event, the particles should not be positioned at positions that result in an appreciable overlap of the atomic or molecular cores. Often this is achieved by initially placing the particles on a cubic lattice [28].

In this place we should introduce the definition of periodic boundary conditions (PBC). Let us consider 1000 atoms arranged in a cube with a volume of 10^3. Nearly half the atoms are on the outer faces, and these will have a large effect on the measured properties. Even for $10^6 = 100^3$ atoms, the surface atoms amount to 6% of the total, which is not negligible. Surrounding the cube with replicas of itself takes care of this problem. Provided the potential range is not too long, we can adopt the minimum image convention - each atom interacts with the nearest atom or image in the periodic array. The cubic box is replicated throughout space to form an infinite lattice. Its periodic image in each of the neighbouring boxes moves exactly in the same way. This is shown in Fig. 3.2. Of course, it is important to bear in mind the imposed artificial periodicity when considering properties which are influenced by long-range correlations. There are no walls at the boundary of the central box, and no surface molecules. Special attention must be paid to the case where the potential range is not short: for example for charged and dipolar systems [32].

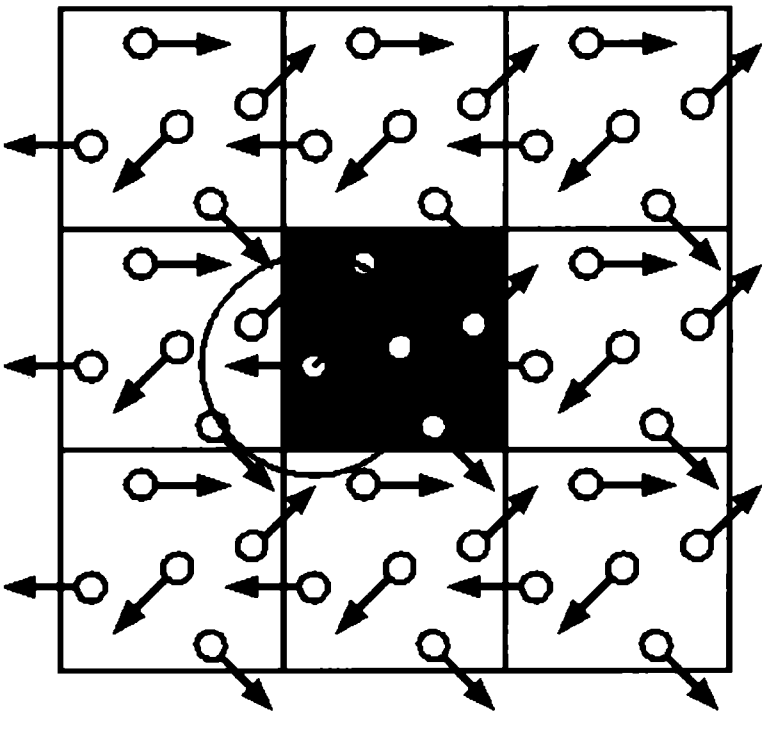

Fig. 3.2 Periodic boundary conditions (PBC)

The calculation of the force acting on every particle is the next basic step and this is the most time-consuming part of almost all molecular dynamics simulations. If we take a model system with pairwise additive interactions, as we do in the present case, we must consider the contribution to the force on particle due to all its neighbours. If we consider only the interaction between a particle and the nearest image of another particle, this implies that, we must evaluate $N\cdot(N-1)/2$ pair distances. If we use no tricks the time needed for the estimation of the forces scales as N^2. There are efficient techniques to speed up the evaluation of both short-range and long-range forces in such a way that the computing time scales as N, rather than N^2. However, in the present example we will not attempt to make the program efficient and we shall, in fact, consider all possible pairs of particles explicitly. Suppose we perform a simulation of a system with short-range interaction potential i.e. the total potential energy of a given particle i is dominated by interactions with neighboring particles that are closer than some cutoff distance r_c. The case that r_c is less than half the diameter of the periodic box is of special interest because in that case we need to consider the interaction of a given particle i only with the nearest periodic image of any other particles j.

In simulations it is often convenient to express quantities such as temperature, density, pressure, etc... in reduced units. Unit systems are constructed to make physical laws look simple and numerical calculations more easy. For the Lennard-Jones system a natural choice of our basic units is the following: σ - unit of length, ε - unit of energy, and m – unit of mass (the mass of the atoms in the system). All other units follow from these basic units. For instance, our unit of time is $\sigma\sqrt{m/\epsilon}$ and the unit of temperature is ε/k_B. In terms of these reduced units the reduced pair potential $V_* = V/\varepsilon$ is a dimensional function of the reduced distance $r_* = r/\sigma$. We get the reduced form for the L-J potential given by

$$V_{*LJ}(r_*)=4\left[\left(\frac{1}{r_*}\right)^{12}-\left(\frac{1}{r_*}\right)^{6}\right] \quad . \tag{3.4}$$

If a given pair of particles is close enough to interact, we have to calculate the force between these particles, and the contribution to the potential energy. If we need to compute the x-component of the force for a Lennard-Jones system (in reduced units) we must find a derivative of L-J potential function with minus sign:

$$F_x(r_*)=-V'_{*LJ}(r_*)=\frac{48x}{r_*^2}\left(\frac{1}{r_*^{12}}-\frac{1}{2r_*^6}\right) \quad . \tag{3.5}$$

We have computed all forces between the particles so in the next step we are going to integrate Newton's equations of motion. A few algorithms have been designed to do this and

one of these will be discussed in a bit more detail; so-called Verlet algorithm. This numerical recipe is not only one of the simplest, but also usually quite good. We should start with a Taylor expansion of the coordinate of a particle, around time t,

$$\vec{r}(t+\Delta t)=\vec{r}(t)+\vec{v}(t)\Delta t+\frac{\vec{F}(t)}{2\mathrm{m}}\Delta t^2+\frac{\Delta t^3}{3!}+O(\Delta t^4) \quad , \tag{3.6}$$

similarly,

$$\vec{r}(t-\Delta t)=\vec{r}(t)-\vec{v}(t)\Delta t+\frac{\vec{F}(t)}{2\mathrm{m}}\Delta t^2-\frac{\Delta t^3}{3!}+O(\Delta t^4) \quad . \tag{3.7}$$

Summing two previous equations, we get

$$\vec{r}(t+\Delta t)+\vec{r}(t-\Delta t)=2\vec{r}(t)+\frac{\vec{F}(t)}{m}\Delta t^2+O(\Delta t^4) \tag{3.8}$$

or

$$\vec{r}(t+\Delta t)=2\vec{r}(t)-\vec{r}(t-\Delta t)+\frac{\vec{F}(t)}{m}\Delta t^2 \tag{3.9}$$

The estimation of the new position contains an error that is of order Δt^4, where Δt is the time step in our molecular dynamics procedure. It is worth noting that the velocities are not needed to compute trajectories because the Verlet algorithm does not use the velocity to predict the new position. The velocity can be derived from knowledge of the trajectory, using

$$\vec{r}(t+\Delta t)-\vec{r}(t-\Delta t)=2\vec{v}(t)\Delta t+O(\Delta t^3) \tag{3.10}$$

$$\vec{v}(t)=\frac{\vec{r}(t+\Delta t)-\vec{r}(t-\Delta t)}{2\Delta t}+O(\Delta t^2) \quad . \tag{3.11}$$

This mathematical expression for the velocity is only accurate to order Δt^2. However, it is possible to obtain more accurate estimations of this physical quantity (and thereby of the kinetic energy) using a Verlet algorithm (an algorithm which yields trajectories identical to that given by equation 3.9). In discussed MD scheme, we use the velocities only to compute the kinetic energy and, thereby, the instantaneous temperature. If we have computed the new positions we may discard the positions at time t - Δt. The current positions become the old positions and the new positions become the current positions. We compute such observables like the current temperature, the current potential energy calculated in the force loop, and the total energy, after each time step. What is important, the total energy should be conserved [28].

3.4 Monte Carlo method

Monte Carlo is one of the major numerical method which was developed by group of researchers (Metropolis, John von Neumann and Stanisław Ulam) in the second half of XX century for estimating multidimensional integrals or solving integral equations. Generally, this computer simulation method is a statistical approach to solve deterministic many-body problems. The fundamental idea of the MC technique is to chose points in the area enclosed by the boundary and then take the weighted data as the estimated value of the integral we are interested in. Early Monte Carlo simulations go back to the 1950s, when such an invention as computer was available. In this section, we will consider a few simple examples to illustrate how a basic Monte Carlo scheme works: numerical estimation of definite integral, evaluation of π value and the Metropolis algorithm.

First, if we need to find the numerical value of the integral

$$S=\int_0^1 f(x)\,dx \tag{3.12}$$

we can divide the region [0, 1] evenly into M pieces with $x_0 = 0$ and $x_M = 1$, and then the integral can be approximated as

$$S=\frac{1}{M}\sum_{n=1}^{M} f(x)+O(h^2) \quad , \tag{3.13}$$

which is equivalent to sampling from a set of points $x_1, x_2, \ldots, x_M$ in the region [0, 1] with an equal weight, in this case, 1, at each point. We can also select x_n with $n = 1, 2, \ldots, M$ from a uniform random number generator in the region [0, 1] to accomplish the same goal. If M is large enough, we would expect x_n to be a set of numbers uniformly distributed in the region [0, 1] with certain fluctuations proportional to factor $1/\sqrt{M}$. Next, the integral can be approximated by the average value obtained from

$$S\simeq\frac{1}{M}\sum_{n=1}^{M} f(x_n) \quad , \tag{3.14}$$

where x_n is a set of M points generated from a uniform random number generator in the region [0, 1]. The possible error in the estimation of the integral is now given by the fluctuation of the distribution x_n. In case of using the standard deviation of statistics to evaluate the possible error of the random sampling, we have

$$(\Delta S)^2=\frac{1}{M}(\langle f_n^2\rangle-\langle f_n\rangle^2) \quad . \tag{3.15}$$

The following formula describes how the average of a quantity is defined

$$\langle A_n \rangle = \frac{1}{M} \sum_{n=1}^{M} A_n \ , \tag{3.16}$$

where A_n is the sampled data [33].

A very good illustration of the use of MC technique is also a method of integration by returning to the evaluation of π. One of the methods is finding the area of the circle of unit radius. The circle inscribed in a square is shown in Fig. 3.2. A number of trial shots are generated in the small square OABC. At each trial two independent numbers are randomly chosen from a uniform distribution on [0,1]. These numbers represent the coordinates of a point and the distance from the origin to the random point is calculated. If this distance is less or equal to one, the shot has landed in the circle area (colorized part of a circle) and a hit is scored. If a total of τ_{shot} are fired and τ_{hit} hits scored then π approximation is given by

$$\pi \approx \frac{4 \cdot Area\ under\ the\ curve}{(Area\ of\ the\ square)} = \frac{4 \cdot \tau_{hit}}{\tau_{shot}} \ . \tag{3.17}$$

Numerical procedure described above is often called hit and miss experiment and can be performed on every computer. If we want to estimate π to four digits we have to run the program with 10^7 shots [30].

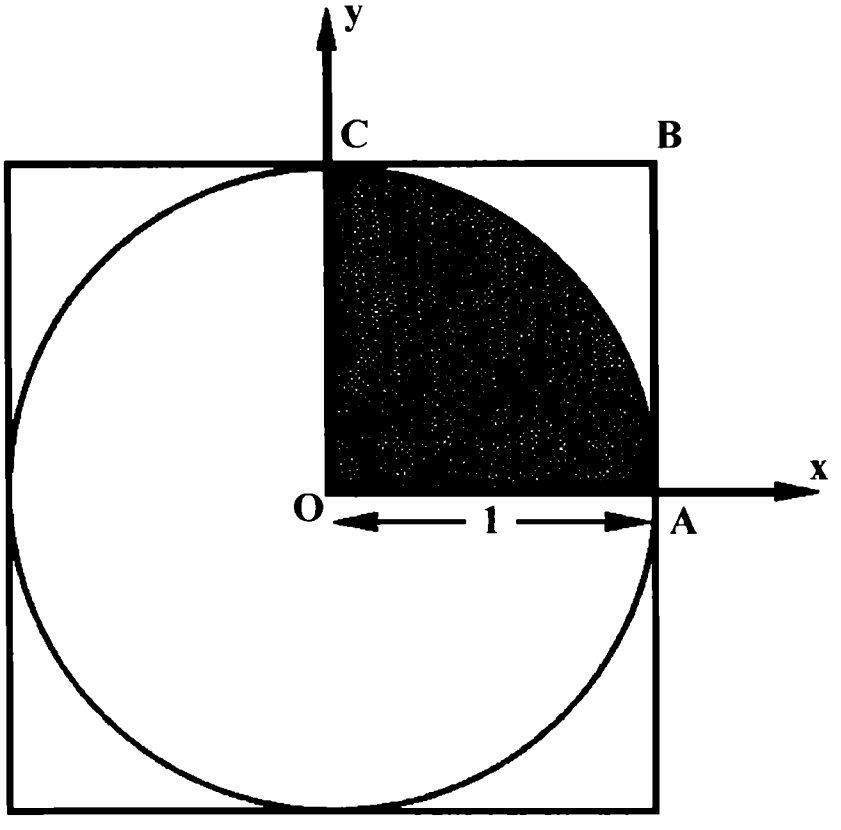

Fig. 3.3 The geometrical model for the hit and miss integration to find the area of the circle

3.4.1 The Metropolis algorithm

When studying systems with many particles, the number of possible configurations becomes unimaginably large very quickly, even for simple binary models, in which each particle may exist in one of two possible states. The number of configurations of such system grows extremely rapidly with the number of particles (N). We may analyse an example of statistical mechanics in which we can divide the room into two equal halves, and inquired into the number of ways of partitioning the N air molecules between the two halves. The same mathematical apparatus describes a simple Ising model of magnetic spins, in which each spin (-1/2) particle may either be „spin up" or „spin down" with respect to a chosen axis. Since each of the N particles may exist in 2 possible states, provided that we can distinguish the particles, the number of configurations is

$$\Omega = 2^N \quad . \tag{3.18}$$

Let us assume a model of a square lattice of such spins with $32 \cdot 32 = 2^{10}$ spins. This is extremely small on the scale of a macroscopic sample of matter but however there are

$$\Omega = 2^{2^{10}} \approx 10^{308} \tag{3.19}$$

different possible configurations of this system. The major postulate of statistical mechanics is that in equilibrium, an isolated system is equally likely to be found in any one of these configurations that is consistent with exemplary macroscopic properties such as volume, number of particles and total magnetic moment. To compute the time-averaged properties one measures experimentally, we instead calculate an ensemble average over all the accessible configurations.

Usually, a system is not energetically isolated from its surroundings, but may exchange energy with them. This exchange is characterized by thermodynamic quantity, a temperature T, which quantifies how easily the environment shares its energy. The greater temperature, the more easily the environment gives energy to the ensemble; the smaller T, the more the environment puts a premium on having the system in a low energy state. The Boltzmann factor, $e^{-E/kT}$, is proportional to the probability P that the system will be found in a particular configuration at energy E when the temperature of the environment is T and k is Boltzman constant. This relationship of proportionality between probability and the Boltzman constant is given below

$$P \propto e^{-E/kT} \quad . \tag{3.20}$$

When the particles don't interact with one another, we are able to manage the sums

analytically; this describes spins in an external magnetic field, ideal gases, lattice vibrations, black body radiation, and other simple systems. If the particles do interact to an appreciable extent, one can almost never perform the sums analytically.

If we want to find an approximation numerically we may use the Metropolis algorithm which is based on the concept of detailed balance that describes equilibrium for systems whose configurations have probability proportional to the Boltzmann factor. We seek to sample the space of possible configurations in a thermal way. It is clear that this way must agree with eq. 3.20. We may achieve this by exploring possible transitions between all configurations. Let us take two configurations A and B, each of which occurs with probability proportional to the Boltzmann factor

$$\frac{P(A)}{P(B)} = \frac{e^{(-E_A/kT)}}{e^{(-E_B/kT)}} = e^{-(E_A - E_B)/kT} \tag{3.21}$$

The formed ratio converts relative probabilities involving an unknown proportionality constant (called the inverse of the partition function) into a pure number. It is written in Metropolis paper [29] that the relative probability of eq. 3.21 can be obtained in a simulation by proceeding as follows:

1. Starting from a configuration A, with known energy E_A, make a change in the configuration to obtain a new configuration B.
2. Compute energy E_B (usually as a small change from E_A).
3. If $E_B < E_A$, assume the new configuration, since it has lower energy (according to the Boltzmann factor).
4. Else ($E_B > E_A$), accept the new (higher energy) configuration with probability $p = exp\ (-(E_B - E_A)/kT)$.
   This can be explained that when the temperature is high, we don't mind taking steps in the „wrong" direction, and as the temperature is lowered, we are forced to settle into the lowest configuration we can find in our neighborhood.

If we use this recipe, then we will sample points in the space of all possible configurations with probability proportional to Boltzman factor $e^{-E/kT}$, consistent with the theory of equilibrium statistical mechanics. Average properties can be computed by summing them along the path we follow through possible configurations [32].

4
COMPUTER SIMULATION MODEL

4.1 Molecular modelling

Molecular modelling techniques encompasse all theoretical and computational methods used to describe molecules and are used in the fields of computational chemistry, biology, physics, etc. . The common feature of these techniques is the atomistic level description of the molecular systems. The lowest level of information is single atoms or a small group of atoms (so-called „superatoms"). This is in contrast to quantum chemistry (electronic structure calculations) where electrons are considered explicitly. Molecular modelling gives very important benefit because it reduces the complexity of the system, allowing many more objects (particles or atoms) to be considered during simulations. When molecules are near enough to interact, we must concern ourselves with the balance between the forces of attraction and repulsion. It is well known that such forces exist, otherwise there would be nothing to bring molecules together into the solid and liquid states, and all matter would be gaseous. A study of the forces between atomic or molecular species constitutes the issue of intermolecular forces [34]. We know there are two main kinds of molecule model: rigid molecule (rigid chemical bonds) and flexible model (elastic bonds). Calculations in this work have been done using two different potentials and all details are described in next subsections.

4.1.1 Rigid bonds

A rigid body (in physics) is an idealization of a solid body of finite size in which the distance between any two given points of a rigid body remains constant in time regardless of external forces exerted on it. Even though such an object cannot physically exist due to relativity, objects can normally be assumed to be perfectly rigid if they are moving much more slowly than speed of light. A rigid body, in classical mechanics, is usually considered as a continuous mass distribution, while in quantum mechanics a rigid body is usually thought of

as a collection of point masses. For example, in quantum mechanics molecules are often seen as rigid bodies.

Fully rigid molecules exist in two forms, linear and nonlinear, with each molecule having two or three rotational degrees of freedom respectively. The orientation of a rodlike linear molecule can be specified using two angular coordinates but more general case requires three. Euler angles are usually introduced as a particularly simple way of describing orientation [31]. Alternatively the orientation can be described by the quaternion - a four dimensional unit vector (q_0, q_1, q_2, q_3). In terms of the Euler angles, the quaternions are defined as

$$q_0=\cos\frac{1}{2}\theta\cos\frac{1}{2}(\phi+\psi) \quad , \tag{4.1}$$

$$q_1=\sin\frac{1}{2}\theta\cos\frac{1}{2}(\phi-\psi) \quad , \tag{4.2}$$

$$q_2=\sin\frac{1}{2}\theta\sin\frac{1}{2}(\phi-\psi) \quad , \tag{4.3}$$

$$q_3=\cos\frac{1}{2}\theta\sin\frac{1}{2}(\phi+\psi) \quad . \tag{4.4}$$

The quaternion scheme is computationally simpler and avoids singularities that appear in the equations of motion for the Euler angles [3θ].

I have chosen the 4-n-pentyl-4'-cyanobiphenyl (5CB) molecule as a typical representative of mesogens. This molecule has been studied extensively both theoretically and experimentally and therefore a large data set is available for confrontation with the results from computer simulation. One reason for this large number of experimental investigations is the convenient temperature range of the nematic phase, namely, from 295.6 to 308.5 *K* [35]. The 5CB molecule was modelled as a rigid body with the aromatic CH, and aliphatic CH_2 and CH_3 groups, where these are treated as single interaction centres, so called united atoms (UA) (Fig. 4.1).

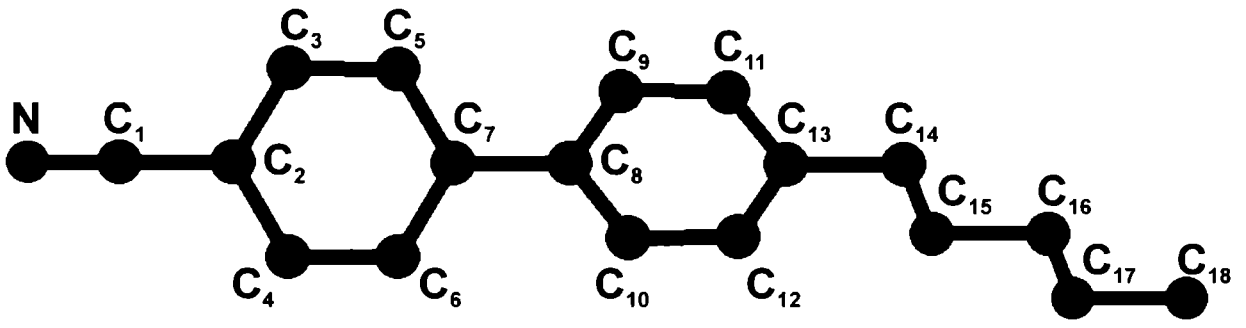

Fig. 4.1 The model of 5CB molecule (without hydrogen atoms)

This operation improves calculation speed because of a reduced number of the interacting sites. The structure and electric charges distribution of 5CB molecule were optimized by the ab initio calculation using the GAMES code [36]. The interaction between each interacting site and supersite in 5CB molecules and carbon nanostructures is described by the sum of the Lennard–Jones and Coulomb potential of the form:

$$V(r_{ij}) = 4\epsilon_{ij}\left[\left(\frac{\sigma_{ij}}{r_{ij}}\right)^{12} - \left(\frac{\sigma_{ij}}{r_{ij}}\right)^{6}\right] + \frac{Z_i Z_j e^2}{4\pi\epsilon_0 r_{ij}} \quad , \tag{4.5}$$

where r_{ij} is the distance between the ith and jth atoms of a pair of different 5CB molecules, Zi, Zj denotes the charges of each site, e is the electron charge. The interaction potential parameters used in the simulation are shown in Table 4.1.

Table 4.1 The potential model parameters of 5CB (taken from [35]) and carbon nanostructure

site	σ_{ii} [nm]	ε_{ii} [$kJ\,mol^{-1}$]	m [u]
N	0.3250	0.72	14.010
C_1	0.3750	0.44	12.000
C_2, C_7, C_8, C_{13}	0.3750	0.46	12.000
C_3-C_6, C_9-C_{12} (CH)	0.3750	0.46	13.008
C_{14} - C_{17} (CH_2)	0.3905	0.50	14.016
C_{18} (CH_3)	0.3905	0.50	15.024
C (CNS)	0.3400	0.44	1.2000

The electric charges distribution of the 5CB molecule model is shown in Table 4.2. I have assumed that there is no electric charge on the carbon structures. The Lennard–Jones potential parameters between unlike atoms A and B are given by Lorentz–Berthelot rules $\sigma_{A-B}=(\sigma_A+\sigma_B)/2$ and $\epsilon_{A-B}=\sqrt{\epsilon_A\epsilon_B}$ [30].

Table 4.2 The distribution of 5CB sites charges (taken from [35])

site	charge $\|e\|$
N	-0.450
C_1	0.100
C_2	0.300
C_3 (CH), C_4 (CH)	-0.075
C_5 (CH), C_6 (CH)	-0.070
C_7	0.250
C_8	0.250
C_9 (CH), C_{10} (CH)	-0.070
C_{11} (CH), C_{12} (CH)	-0.060
C_{13}	0.100
C_{14} - C_{17} (CH_2), C_{18} (CH_3)	0

4.1.2 Elastic bonds

The study of molecules with elastic bonds has been one of the main areas of interest during the last years [35, 37-40] . For instance such molecules like n-butane do not have a rigid permanent shape. In fact they may adopt many different shapes or conformations. For example n-butane can exist in the spacial configuration denoted as trans (where all C atoms are in a plane) or in the spatial configuration denoted as gauche (where one of the C atoms is out of the plane). In a liquid sample of a fluid with flexible molecules such as n-hexane some particles adopt the all trans configuration, other adopt a configuration with all bonds in trans configuration but one in the gauche configuration etc. The spatial molecular shape is dynamic in the sense that a given molecule adopt a number of different spatial configurations in time. Alkanes are well known and typical example of a flexible molecules.

The 5CB mesogens were also treated as flexible and modelled by CHARMM 27 force field [41], which includes intramolecular harmonic stretching, harmonic bending, torsional,

van der Waals and Coulombic terms. The form of the potential energy function is given by the following equation:

$$V_{total} = V_{stretch} + V_{bend} + V_{vdW} + V_{Coulomb} + V_{torsional} \quad , \tag{4.6}$$

$$V_{total} = K_r(r - r_0)^2 + K_\Theta(\Theta - \Theta_0)^2 + 4\epsilon\left[\left(\frac{\sigma}{r}\right)^{12} - \left(\frac{\sigma}{r}\right)^{6}\right] + \frac{e^2}{4\pi\epsilon_0 r} + \begin{cases} K_\phi(1 + \cos(n\phi - \gamma)), n \neq 0 \\ K_\phi(\phi - \gamma)^2, n = 0 \end{cases} \tag{4.7}$$

The use of full atomistic potentials, which include all hydrogens, is very demanding in terms of computer resources, and it is worth asking if a slightly smaller resolution, such as that afforded by the united-atom (UA) approximation [30], where CH, CH_2 and CH_3 groups are considered as suitably parameterized spherical interaction sites.

Table 4.3 Description of atoms forming 5CB mesogenic molecule and carbon nanostructures

Atom type	site	description
N	N	sp nitrogen
C0	C_1	sp carbon without hydrogens
C00	C_2, C_7, C_8, C_{13}	sp^2 carbon without hydrogens
C1	C_3-C_6, C_9-C_{12}	sp^2 carbon with 1 hydrogen
C2	C_{14} - C_{17}	sp^3 carbon with 2 hydrogens
C3	C_{18}	sp^3 carbon with 3 hydrogens
C (CNS)	C	aromatic sp^2 carbon (from carbon nanostructure)

Carbon nanostructures (nanotube, graphite and graphene) have also been modelled using flexible model based on CHARMM 27 force field.

Interactions between CNS and 5CB molecules have been described by usual Lennard-Jones 12-6 potential with Lorentz-Berthelot mixing rules. Specification of the force field parameters for all interactions are given in Table 4.4. Charge distribution on 4-n-pentyl-4'-cyanobiphenyl mesogen has been calculated on ab initio level and is presented in Table 4.5. Similar to rigid model, which is described in previous subsection in details, there is no electric charge on carbon atoms of CNS (nanotube, graphite, graphene).

Table 4.4 CHARMM force field parameters for 5CB (taken from [40]) and carbon nanostructures

Stretching type		
$V_{stretch}=K_r(r-r_0)^2$	K_r [*kcal mol*$^{-1}$ Å^{-2}]	r_0 [Å]
C00-C0	95.9	1.42
C1-C1	469.0	1.41
C00-C1	469.0	1.41
C00-C00	469.0	1.48
C2-C2	95.9	1.54
C2-C3	95.9	1.54
C0-N	600.00	1.16
C00-C2	317.0	1.51
C-C (CNS)	305.0	1.38
Bending type		
$V_{bend}=K_\Theta(\Theta-\Theta_0)^2$	K_Θ [*kcal mol*$^{-1}$ *rad*$^{-2}$]	Θ_0 [degrees]
C2-C2-C2	63.0	112.4
C2-C2-C3	62.1	114.0
C3-C2-C3	62.1	114.0
C00-C00-C1	85.0	120.0
C1-C00-C1	85.0	120.0
C00-C1-C1	85.0	120.0
CY-C00-C1	85.0	120.0
C00-C0-N	79.5	180.0
C1-C00-C2	70.0	120.0
C00-C2-C2	63.0	112.4
C-C-C (CNS)	40.0	120.0
Torsion type		
$V_{torsional}=\begin{cases}K_\phi(1+\cos(n\phi-\gamma)), n\neq 0\\ K_\phi(\phi-\gamma)^2, n=0\end{cases}$	K_Φ [*kcal mol*$^{-1}$]	n	γ [degrees]
C00-C1	2.65	2	180.0
C1-C1	5.3	2	180.0
C2-C00	0,5	6	0.0
N-C0-C00-C1	0.0	1	180.0
C2-C2	0.6706	1	0.0
C2-C2	0.1365	2	0.0
C2-C2	1.4	3	0.0

C00-C00	0.010	1	180.0
C00-C00	0.692	2	180.0
C00-C00	0.001	3	180.0
C00-C00	1.064	4	0.0
C-C-C-C (CNS)	3.1	2	180.0

van der Waals type			
$V_{vdW}=4\epsilon[(\sigma/r)^{12}-(\sigma/r)^{6}]$	ϵ [$kcal\ mol^{-1}$]	$2^{1/6}\sigma/2$ [Å]	m [u]
N	-0.1700	1.824	14.010
C0	-0.0860	1.908	12.000
C00	-0.708	1.950	12.000
C1	-0.708	1.950	13.008
C2	-0.0705	2.035	14.016
C3	-0.1050	2.050	15.024
C (CNS)	-0.0700	1.992400	1.2000

Table 4.5 Charge distribution on 5CB molecule (charges are given in electrostatic units)

site	charge $\|e\|$
N	-0.559
C_1	0.767
C_2	-0.804
C_3 (CH), C_4 (CH)	0.242
C_5 (CH), C_6 (CH)	0.156
C_7	-0.211
C_8	-0.330
C_9 (CH), C_{10} (CH)	0.150
C_{11} (CH), C_{12} (CH)	0.196
C_{13}	-0.640
C_{14} (CH_2)	0.286
C_{15} (CH_2)	0.030
C_{16} (CH_2)	-0.056
C_{17} (CH_2)	0.030
C_{18} (CH_3)	-0.004

4.2 Description of calculated observables

Physical properties of 5CB mesogens were studied by calculating several dynamical and structural characteristics. All these observables give us many useful information about investigated molecular system. Numerical and mathematical procedures are described in two subsections (4.2.1 and 4.2.2). All algorithms for basic data analyse from molecular dynamics trajectories were implemented in C++ programming language.

4.2.1 Dynamical properties

Dynamical observables are used to investigate physical properties of samples. Numerical methods with visualization let us better understand and explain basic properties.

We know there are two types of velocity of molecule: linear $\vec{v}$ and angular $\vec{\omega}$. To obtain physically meaningful information basing on these observables, it is convenient to calculate the velocity autocorrelation function (VACF):

$$C_v(t)=\frac{\langle \vec{v}(t)\cdot\vec{v}(0)\rangle}{\langle \vec{v}(0)^2\rangle}\ , \tag{4.8}$$

$$C_\omega(t)=\frac{\langle \vec{\omega}(t)\cdot\vec{\omega}(0)\rangle}{\langle \vec{\omega}(0)^2\rangle}\ , \tag{4.9}$$

where <...> represents average over time and molecules in the ensamble.

These functions are of great interest in computer simulation because of a following reasons:

(1) they give a very clear picture of the dynamics in fluids;

(2) their time integrals may almost always be related directly to macroscopic transport coefficient;

(3) their Fourier transforms may usually be related to experimental spectra [30].

The thermal motion of molecules in liquid or gas phase is often described as a diffusion process. Diffusion of a labeled species among otherwise identical molecules is called self-diffusion. The translational diffusion coefficient D shows how fast that phenomena occurs and is directly connected with the mean square displacement $\langle|\Delta r(t)|^2\rangle=\langle|\vec{r}(t)-\vec{r}(0)|^2\rangle$.

D is a macroscopic transport coefficient and $\langle \vec{r}^2(t)\rangle$ has a microscopic interpretation: it is the mean-squared distance over which the labeled molecules have moved in a time interval t.

One way to get a value of diffusion coefficient is integrating the VACF like below:

$$D=\frac{1}{3}\int_0^\infty \langle \vec{v}_i(t)\cdot\vec{v}_i(0)\rangle dt \quad , \tag{4.10}$$

where $\vec{v}_i(t)$ is the centre of mass velocity of a single molecule. Einstein relation, valid at long times, is another way to compute D

$$2\,Dt=\frac{1}{3}\langle|\vec{r}_i(t)-\vec{r}_i(0)|^2\rangle \quad , \tag{4.11}$$

$$\langle|\Delta r(t)^2|\rangle\simeq 6\,Dt \quad , \tag{4.12}$$

where $\vec{r}_i(t)$ is the molecule position.

The information about the dipolar relaxation can be obtained from MD trajectories in the form of the normalized total dipole moment time correlation function (TCF) defined as [42]

$$C(t)=\frac{\langle \vec{M}(t)\cdot\vec{M}(0)\rangle}{\langle \vec{M}(0)^2\rangle} \quad , \tag{4.13}$$

$$\vec{M}(t)=\sum_{n=1}^{N}\vec{\mu}_i(t) \quad , \tag{4.14}$$

where N is the total number of molecules, and $\vec{\mu}_i$ is the dipole moment of the ith molecule. The connection between the frequency domain dielectric permittivity

$$\epsilon(\omega)=\epsilon'(\omega)-i\epsilon''(\omega) \quad , \tag{4.15}$$

which can be measured in the frequency domain dielectric spectroscopy experiments, and the total dipole moment time correlation function can be introduced as follows:

$$\epsilon'(\omega)=\epsilon_0-(\epsilon_0-\epsilon_\infty)\omega\int_0^\infty \phi(t)\sin\omega t\,dt \quad , \tag{4.16}$$

$$\epsilon''(\omega)=(\epsilon_0-\epsilon_\infty)\omega\int_0^\infty \phi(t)\cos\omega t\,dt \quad , \tag{4.17}$$

where $\varepsilon'(\omega)$ is the real part (permittivity factor) and $\varepsilon''(\omega)$ is imaginary (dielectric loss) part [43].

4.2.2 Structural properties

A second class of observables are the functions that characterize the local structure of a nanomaterial. Most notable among these is the so-called radial distribution function $g(r)$ (RDF). This function gives the probability of finding a pair of atoms a distance r apart relative

to the probability expected for a completely random distribution at the same density [44]. RDF (pair correlation function) describes how the density varies as a function of the distance from a reference particle.

In this dissertation the structure of liquid crystal layers was examined by the radial distribution function

$$g(r)=\int_{r}^{r+dr} 4\pi\xi^2 p(\xi)d\xi \quad , \tag{4.18}$$

calculated as histogram of probabilities $p(\xi)$ of finding other molecules in the sphere of the radius between $r + dr$.

As we well know (discussion in chapter 1.4) the characterization of a liquid crystalline phase inevitably deals with the investigation of its orientational order, and more generally, with the anisotropy of its physical properties. In case of a rigid molecule this is determined by a non-isotropic distribution of molecular orientations $f(\alpha, \beta, \gamma)$. If we take director frame as laboratory frame, the distribution becomes independent of the Euler angle α [45], and if we assume molecular uniaxiality, also from γ, that is, $f = f(\beta)$. To calculate $f(\beta)$, the necessary step is to determine the director at each successive time frame t considered in the MD trajectory [46], and this can be done by setting up and diagonalizing an ordering matrix, Q, given by following equation

$$Q(t)=\sum_{l=1}^{N} [3u_l(t) \otimes u_l(t) - I] / 2N, \tag{4.19}$$

where $u_l(t)$ is the chosen molecular reference axis, I is the identity matrix and the sum runs over all the N molecules of the sample. The instantaneous order parameter $P_2(t)$ can be obtained from the eigenvalues $\lambda_{min} < \lambda_0 < \lambda_{max}$ of the cartesian ordering matrix $Q(t)$ and this is suitable observable for describing the nematic–isotropic phase transition. The typical method is using the largest eigenvalue and identify it as the order parameter: $P_2(t) = \lambda_{max}(t)$. This is a strictly non-negative value, since $Q(t)$ is traceless, so to avoid unrealistically high values of the order parameter in the isotropic phase, $P_2(t)$ is preferably calculated as $P_2(t) = -2\lambda_0(t)$ [47]. The momentary eigenvalues of ordering matrix can be averaged over a sufficiently long and equilibrated trajectory (indicated by angular brackets), to give the uniaxial order parameter

$$\langle P_2 \rangle = \langle P_2(t) \rangle = \langle -2\lambda_0(t) \rangle \tag{4.20}$$

Other way of averaging uses the eigenvectors of $Q(t)$ that provide the instantaneous director frame for the configuration at time t for calculating the Euler angle β between the phase director and the reference axis of molecule i. This allows to compute of the overall average of any function of β, and in particular of the second rank Legendre polynomial [40], yielding the

corresponding order parameter given by formula

$$\langle P_2 \rangle = \left\langle \frac{1}{N} \sum_{i=1}^{N} (3\cos^2\beta - 1)/2 \right\rangle \quad . \tag{4.21}$$

5
RESULTS

During research I have performed many computer simulations of nanosystems. I decided to present results which seem to be the most interesting and give theoretical fundamentals for further developing of main thesis. Every investigated ensemble contains liquid crystal cluster consisted of 5CB molecules (22 – 98 molecules), often located near carbon nanostructure (nanotube, graphite, graphene). The size of the sample depends on kind of carbon nanostructure used in MD simulation. Molecular structure and modelling was described in previous section and description of computer simulation details is given below.

Simulations were started from the first principle calculation of molecule geometry. The calculations were done with GAMES application on the DFT/B3LYP theory level with 6-31G* basis set. For rigid molecule model the classical equations of motion were solved by the Adams-Moulton predictor-corrector algorithm [31]. The integration time step used in the simulations was 1 *fs* which ensures total energy conservation within 0.04%. The system was equilibrated to the desired temperature by the Berendsen thermostat [31] for 10^6 MD steps and the thermostat was switched off during the collection of MD data. The initial positions were generated by the Monte Carlo method [28]. All calculations were carried out for the NVT ensemble.

In other case (flexible bonds) classical equations of motion have been integrated using Brunger-Brooks-Karplus (BBK) method [48] implemented in NAMD [49], with the time step of integration of equations of motion 1 *fs*. Similar to rigid bonds model simulations were also performed in NVT ensemble but the temperature was controlled using Langevin thermostat.

5.1 Free cluster $(5CB)_{22}$

The molecular dynamics (MD) was used to investigate the nano droplet composed of twenty two mesogen molecules 4-n-pentyl-4'-cyanobiphenyl. The mesogens were treated as rigid bodies with no internal degrees of freedom. Before each trajectory production, the system was equilibrated for 1 *ns*. The classical equations of motion were integrated up to 5 *ns* for each temperatue. The trajectory data was collected every 50 time steps.

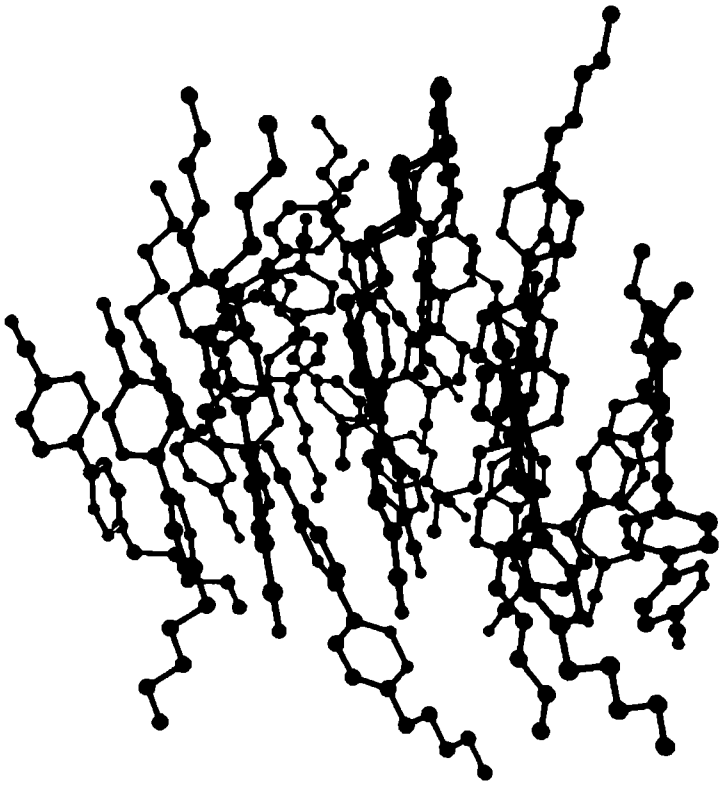

Fig. 5.1 The snapshot of the simulated system at a temperature 150 *K*

A representative snapshot of the instantaneous configuration of $(5CB)_{22}$ at $T = 150$ *K* is shown in Fig. 5.1 which reveals evident spatial ordering of the cluster of mesogen molecules. Their long axes of symmetry are arranged in more or less similar, apparently correlated directions. To check the level of molecular order in the cluster I calculated value of the second rank order parameter $<P_2>$ (see Table 5.1)

Table 5.1 Order parameter $<P_2>$ of $(5CB)_{22}$ cluster for three temperatures

$<P_2>$	temperature [*K*]
0.36	150
0.31	300
0.27	350

The plot of the mean square displacement of mesogen molecule in $(5CB)_{22}$ cluster is shown in Fig. 5.2, where *r* is the position of the mass centre of 5CB.

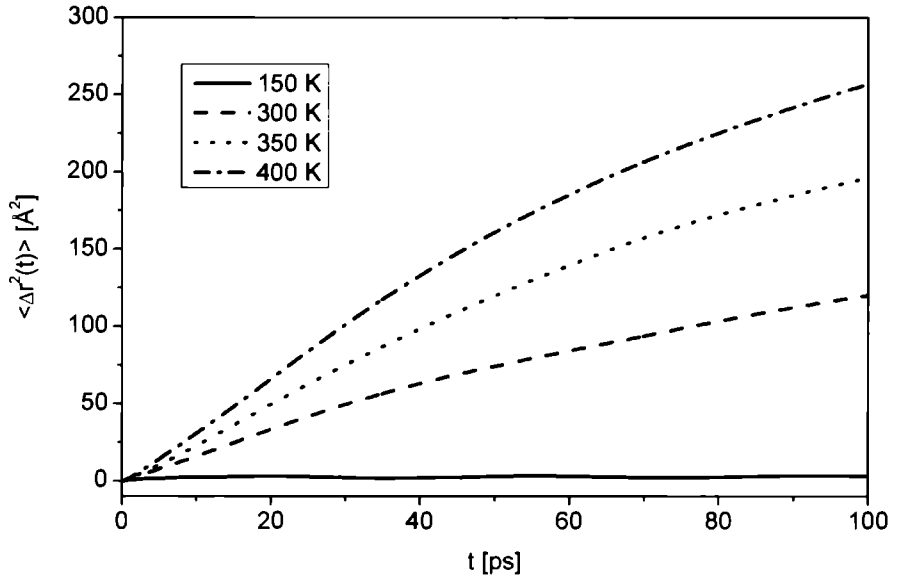

Fig. 5.2 The short-time part of the mean square displacement of the mass centre of 5CB molecule at several temperatures

One can see that at 150 *K* the solid phase of the cluster exists whereas at higher temperatures the translational diffusion of molecules occurs. The diffusion coefficient was either obtain using Einstein relation for $T = 300\ K$ ($D = 0.37 \cdot 10^{-6}\ cm^2/s$), 400 K ($D = 1.73 \cdot 10^{-6}\ cm^2/s$). The soft, spatially ordered phase of mesogen molecules means a liquid crystalline phase.

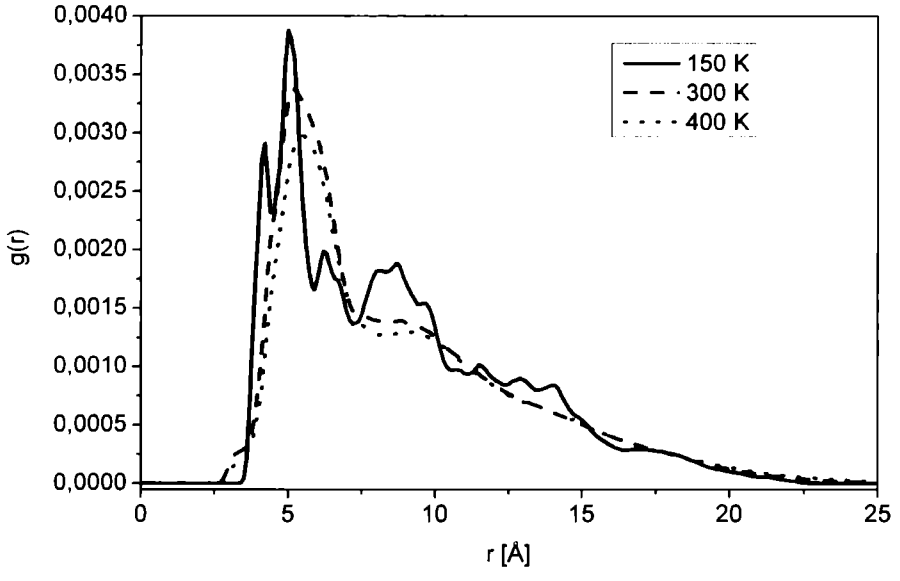

Fig. 5.3 The radial distribution function of 5CB mesogen in $(5CB)_{22}$ cluster, at several temperatures

The radial distribution function $g(r)$ of the mass centre of the 5CB molecule is present as a Fig. 5.3. The appearance of sharp peak at 150 K confirms the solid state of the cluster, for higher temperatures the distribution becomes much broader, characteristic for soft matter, the liquid phase.

To obtain further insight into mesogen dynamics the normalized autocorrelation function $C_v(t)$ was calculated. Fig. 5.4 shows that – in spite of the huge mass of the 5CB molecule – its velocity changes rapidly, being almost entirely decorrelated after 2 *ps*. The oscillations of VACF characteristic for the solid phase disappear at higher temperatures.

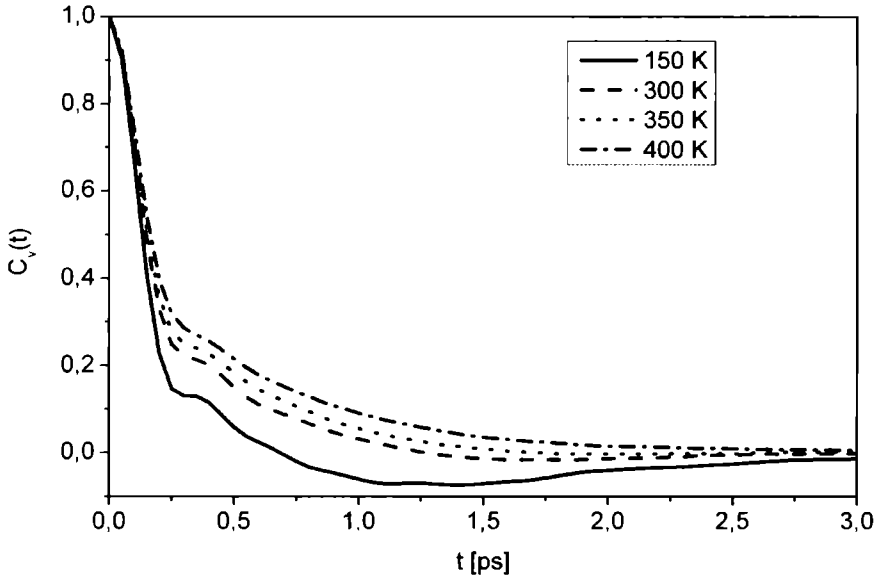

Fig. 5.4 The translational velocity autocorrelation function of 5CB molecule at several temperatures

The angular velocity autocorrelation function $C_\omega(t)$ presented in Fig. 5.5 , decays even faster than $C_v(t)$. The negative dip at t = 0.3 *ps* (T = 300 K) almost vanishes at T = 400 K. Overall, this function changes with temperature, the lower the temperature the greater is the dip of $C_\omega(t)$.

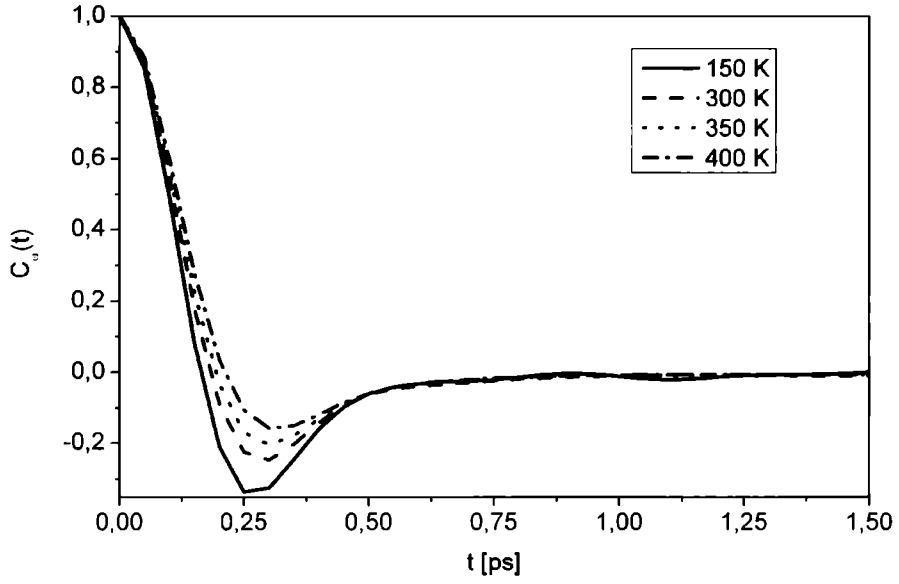

Fig. 5.5 The angular velocity autocorrelation function of 5CB molecule in the cluster, at several temperatures

In a standard dielectric experiment the frequency dependence of the dielectric loss ε''(ω) , which is the imaginary part of complex dielectric permittivity [43] is measured. In case of pure dipolar absorption in the classical limit ($i\hbar \to 0$) ε''(ω) is related to the cosine Fourier transform of the total dipole moment $\vec{M}(t)$ autocorrelation function.

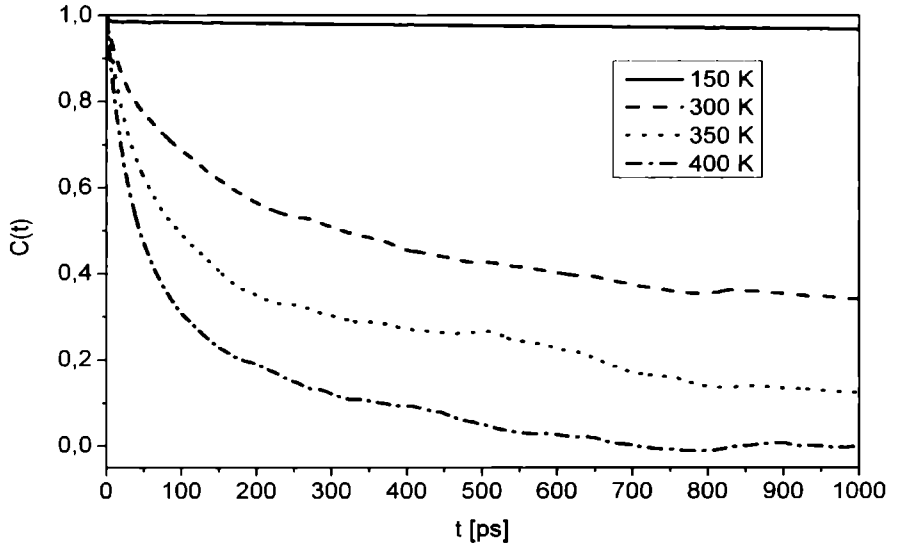

Fig. 5.6 The total dipole moment autocorrelation function of $(5CB)_{22}$ cluster

The normalized correlation function $C(t)$ of investigated sample at several temperatures is shown in Fig. 5.6. The correlation function $C(t)$ is significantly dependent on the temperature. The higher temperature of the system, the faster is the dipolar relaxation, because mesogen molecules encounter more vigorous motion within the cluster. The next Fig. 5.7 presents the simulated normalized dielectric loss of the 5CB cluster. The sensitivity of ε'' to temperature change is clearly observed. The higher the temperature, the greater is the absorption as a result of the increasing mobility of 5CB molecules. The maximum dielectric loss of $(5CB)_{22}$ cluster in the vicinity of frequency region $\nu_{max} \approx 5 \cdot 10^{10}$ *Hz* [50].

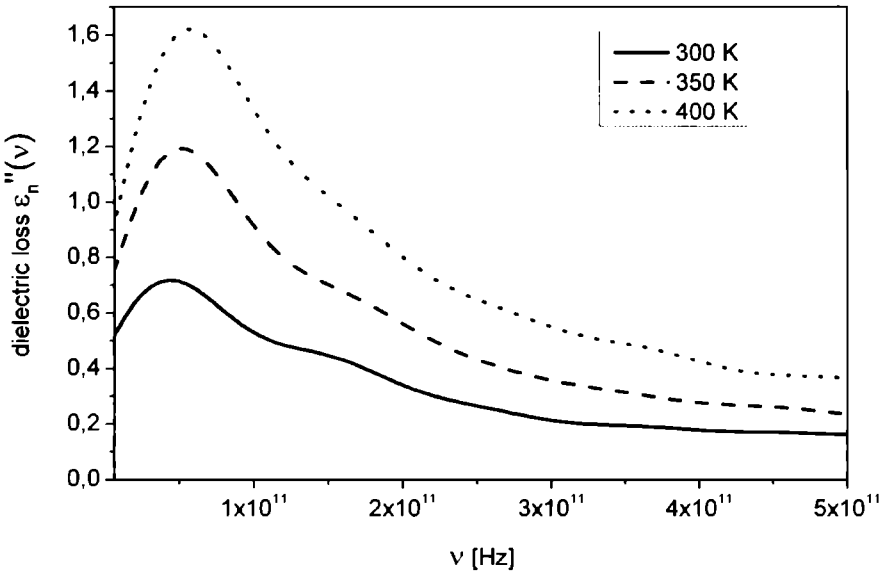

Fig. 5.7 The normalized dielectric loss of $(5CB)_{22}$ cluster

5.2 Carbon nanotube covered by 5CB monolayer

In next part of this work what I aim to do is to present dynamics of mesogen (5CB) thin layer surrounding single-walled, open-ended carbon nanotube (SWCNT) for wide spectrum of temperature. As a typical representative family of carbon nanotubes I have chosen the armchair (10,10) nanotube of the length of 7.5 *nm*. The Lennard-Jones parameters have been set as $\varepsilon/k_b = 28$ *K*, $\sigma = 0.34$ *nm* for carbon taken from [30, 51]. It has been checked that this nanotube can be evenly covered with a single layer composed of twenty two 5CB molecules (for larger number of 5CB mesogens the double layer begins to form). The liquid

crystal molecules spread up to 3.5 nm over the nanotube surface.

An ensemble of mesogenic molecules adsorbed on the surface of SWCNT of different chiralities has been simulated too. The influence of the geometry of a carbon nanotube on the mesogen layer arrangement has been investigated. I have been interested how the structure and dynamics of such ultrathin layer change with the chirality of SWCNTs. The parameters of performed simulation are the same like in previous subsection (free cluster).

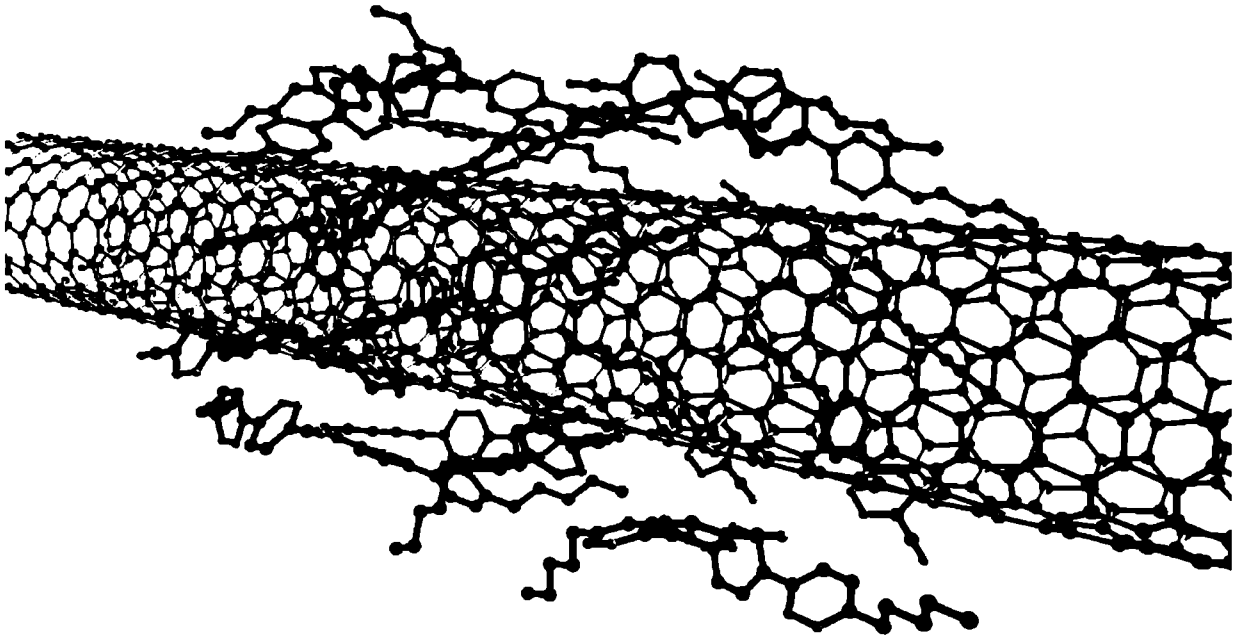

Fig. 5.8 The equilibrium configuration of $(5CB)_{22}$ + nanotube system at $T = 300\ K$

Properties of 5CB layer for a range of temperatures $300\ K < T < 450\ K$ have been studied (using computer simulation technique). An example of the equilibrium configuration of $(5CB)_{22}$ + nanotube system at room temperature is presented in Fig. 5.8. The calculated short-time part of the mean square displacement of 5CB is presented in Fig. 5.9. The slope of the mean square displacement can be directly connected with the translational diffusion coefficient D of a molecule via Einstein formula. The graph of MSD shows the appearance of a liquid phase of 5CB ultrafilm, because the slope of $\langle|\Delta r(t)^2|\rangle \neq 0$ for all temperatures studied. The calculated translational diffusion coefficient of the mass centre of 5CB molecule is: $D = 1.23 \cdot 10^{-6}$, $2.44 \cdot 10^{-6}$, $4.79 \cdot 10^{-6}$, and $7.94 \cdot 10^{-6}\ cm^2/s$ for $T = 300$, 350, 400 and 450 K, respectively.

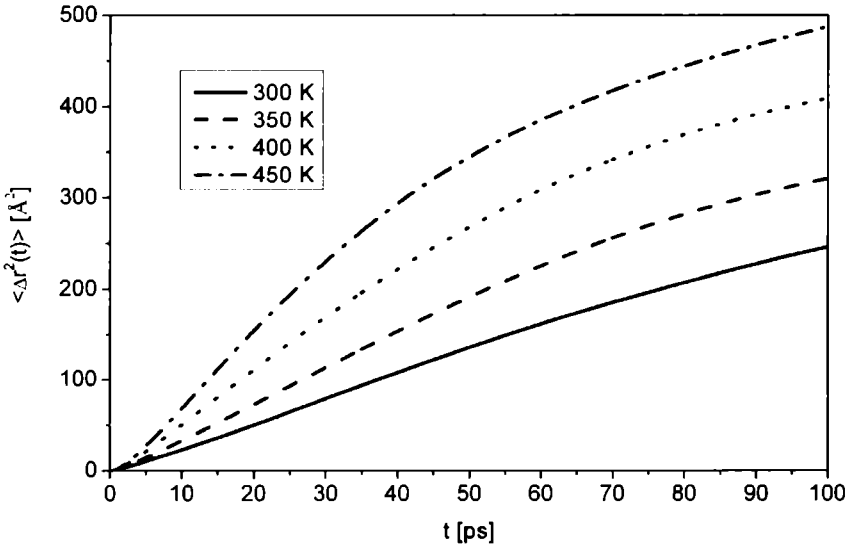

Fig. 5.9 The short-time part of the mean square displacement of the centre of mass of 5CB molecule at several temperatures

The next calculated observable is the normalized velocity autocorrelation function. One can see (Fig. 5.10) that, overall, $C_v(t)$ exhibits the deep dip at $t_d \approx 0.3$ *ps* and dumped pulsations, characteristic for dense phase. The estimated frequency of dumped pulsation is $\nu_{osc} \approx 1.6 \cdot 10^{12}$ *Hz* and it only slightly depends on temperature.

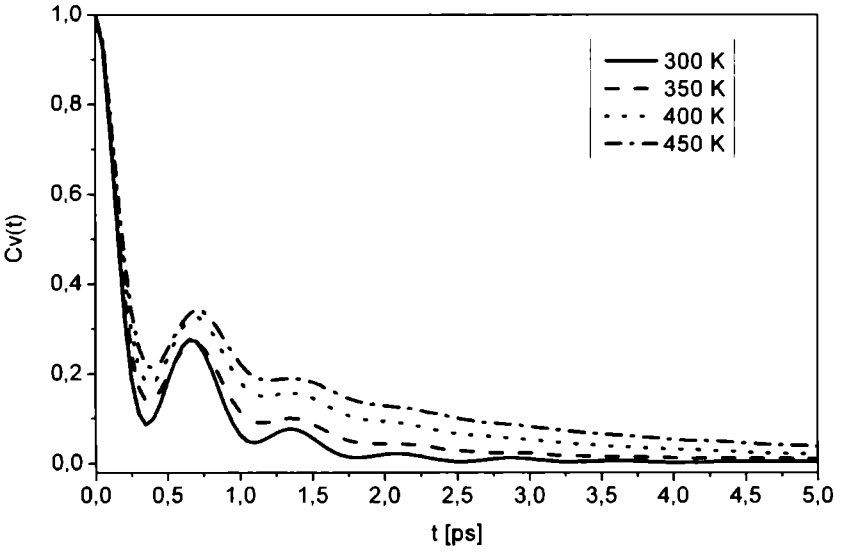

Fig. 5.10 The translational velocity autocorrelation function of 5CB molecule at several temperatures

The modulation of velocity can be attributed to the fast oscillations (librations) of 5CB towards nanotube and back (perpendicular to nanotube's surface). This conclusion is supported by the slight dependence of v_{osc} on temperature. The collisions with neighbouring molecules within the layer would be the alternative source of velocity modulation. However, this process (intermolecular collisions) should be more sensitive to the temperature change and this is not the case.

Another component of translational motion of 5CB molecule is the translocation along nanotube. However the "skating" of a particular 5CB molecule on its way along nanotube is hindered by the collisions with other molecules as well as the attractive influence of nanotube surface. Hence, this is a much slower process, comparing to the "bumping" of 5CB over nanotube and much longer simulation would be required to study this phenomenon. The calculated angular velocity autocorrelation function is shown in Fig. 5.11. This function exhibits also the oscillatory, strongly damped pulsations, characteristic for hindered rotations in dense phase. The negative dip of $C_\omega(t)$ near $t \approx 0.6$ *ps* approximately coincides with its counterpart of $C_v(t)$ (compare Fig. 5.10 and Fig. 5.11).

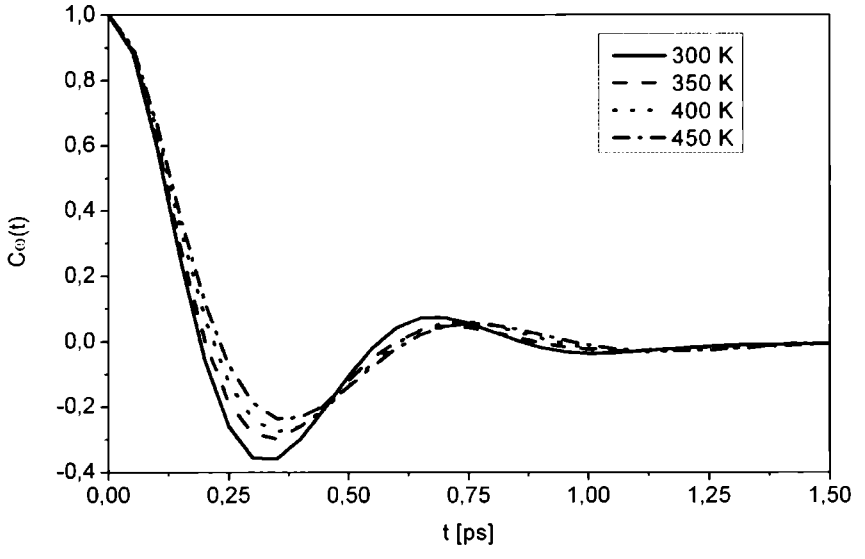

Fig. 5.11 The angular velocity autocorrelation function of 5CB molecule at several temperatures

Therefore, the translational displacement of 5CB mesogen towards nanotube (or back) accompanied by its reorientation, which seems to be natural. The normalized correlation function $C(t)$ of 5CB monolayer at several temperatures is presented in Fig. 5.12. The correlation function significantly depends on temperature what is clearly visible on presented

graph.

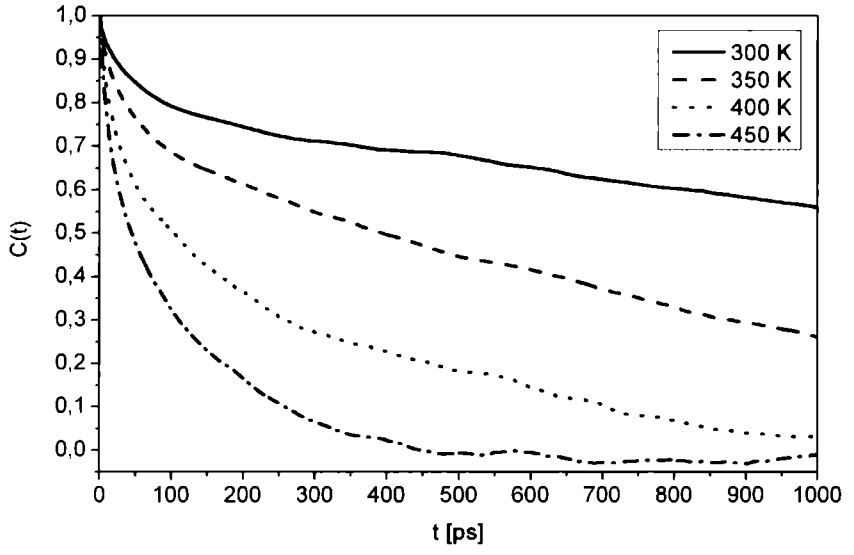

Fig. 5.12 The total dipole moment autocorrelation function of 5CB layer surrounding carbon nanotube

The difference of dielectric relaxation between $(5CB)_{22}$ monolayer covering carbon nanotube and the free cluster is shown in Fig. 5.13. One can see that the same temperature ($T = 300\ K$, room temperature) the dipolar time-correlation function $C(t)$ decays much faster in a free cluster, comparing to its counterpart in monolayer.

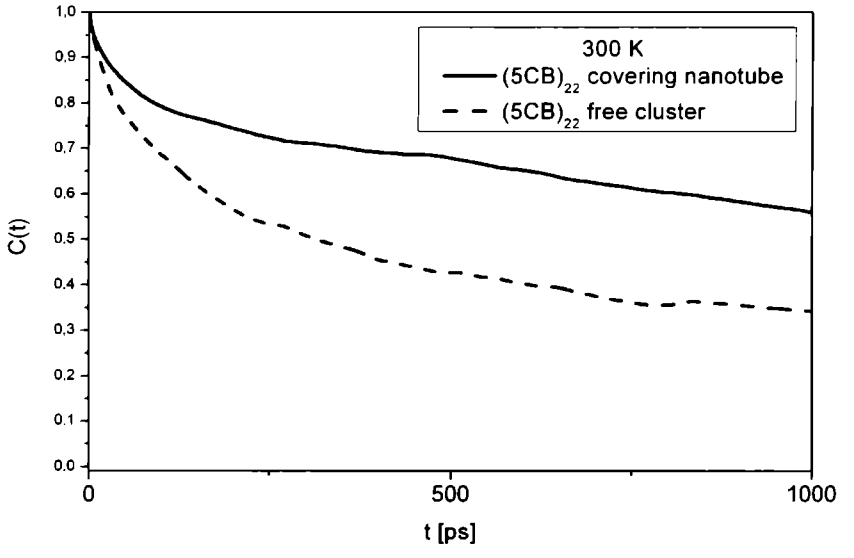

Fig. 5.13 The total dipole moment correlation functions of $(5CB)_{22}$ layer covering carbon nanotube and free $(5CB)_{22}$ cluster at T = 300 *K*

It reflects the fact, that mobility of mesogen molecules in thin film is more restricted by interaction with carbon nanotube surface [52].

Several structural and dynamical characteristics of mesogens covering SWCNTs of different chiralities have been calculated: the radial distribution function, the orientational distribution functions, the angular and linear velocity autocorrelation functions.

The nanotube is characterized by chirality vector $\vec{C}_h = n\vec{a}_1 + m\vec{a}_2$, where n and m are the integer multipliers, $\vec{a}_1$ and $\vec{a}_2$ are the primitive vectors of a graphene unit cell. The diameters of nanotube were calculated from the following formula:

$$d = a_{C-C}\frac{\sqrt{3(n^2+n\cdot m+m^2)}}{\pi} \quad , \tag{5.1}$$

where a_{C-C} is a carbon-carbon bond length [53].

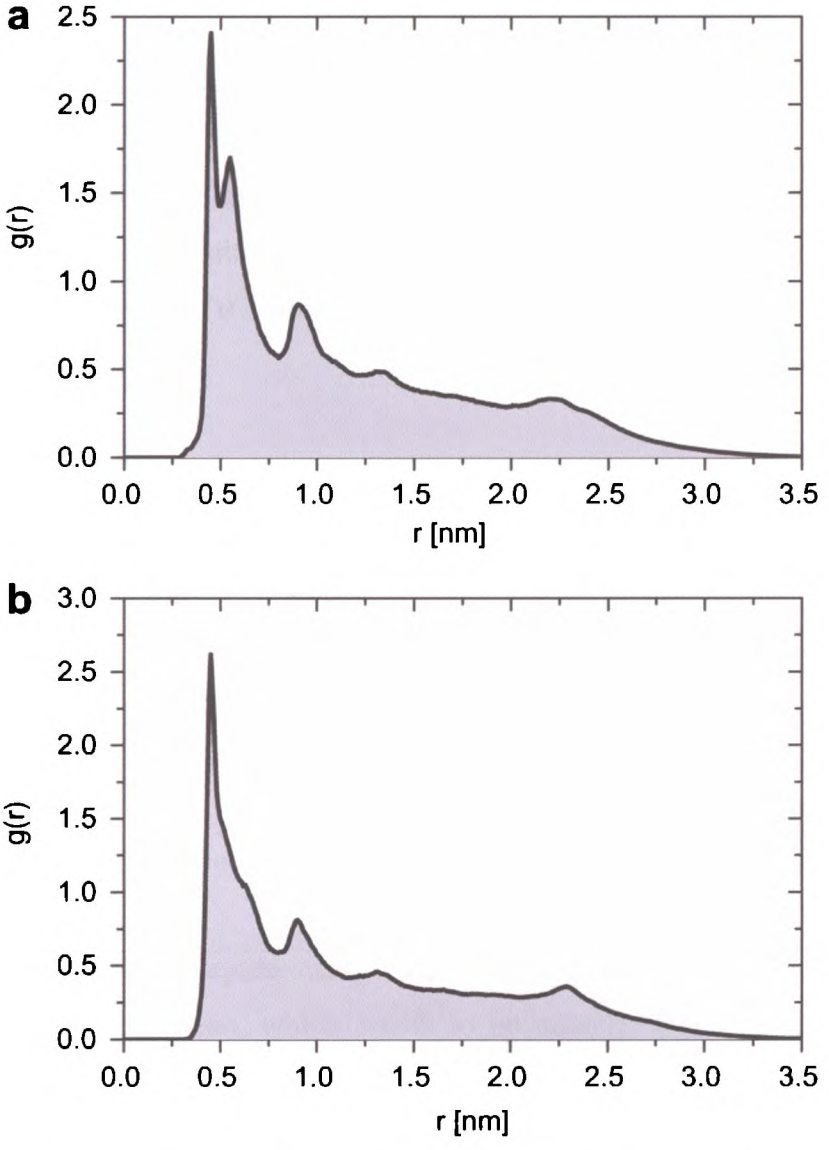

Fig. 5.14 Radial distribution function $g(r)$ of chirality vectors a) (10, 10), and b) (18, 0) at $T = 300\ K$

The chiralities of carbon nanotubes, used in simulations, were chosen to fulfill the constant diameter condition $d \approx 1.4\ nm$. All simulations were carried out in the room temperature ($T = 300\ K$).

The structure of liquid crystalline layer was examined by the radial distribution function $g(r)$. This function for armchair (10,10) nanotube revealed a split of nearest neighbours peak (Fig. 5.14 a) whereas there was no split of this peak in case of the chiral (18, 0) nanotube (Fig. 5.14 b). Two typical alignments of the near neighbour 5CB molecules are shown in Fig. 5.15 and both appear in case of the armchair (10, 10) nanotube. Hence, to near neighbour centre of mass distances show up and this leads to a split of the first $g(r)$ peak. In case of the zigzag chiral nanotube (18, 0) the mesogens tend to follow the nanotubes "pitch".

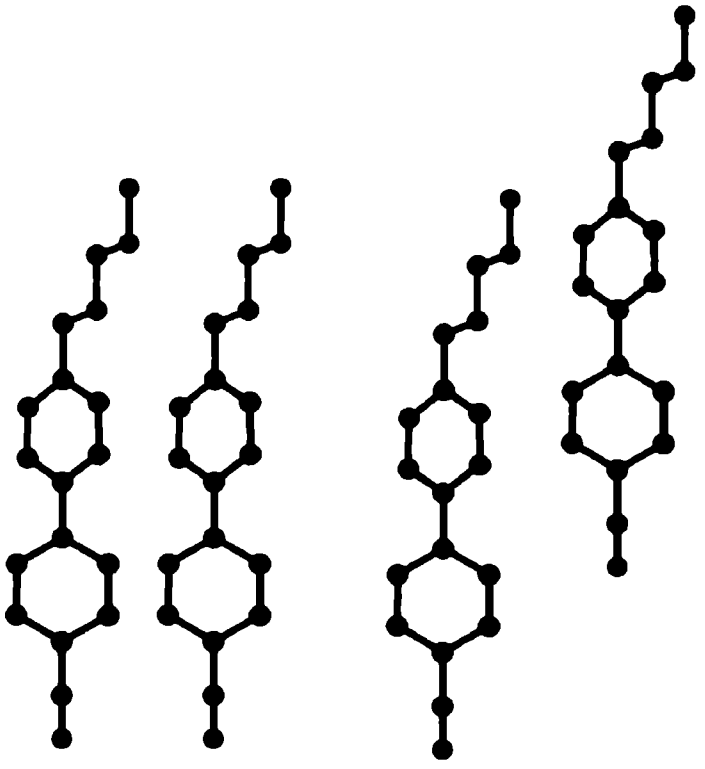

Fig. 5.15 Two typical alignments of the near neighbor 5CB molecules in the ultrathin layer surrounding the armchair (10, 10) nanotube

Next, I calculated the ordering of molecules with respect to director n. The director was estimated as the biggest eigenvalue eigenvector of the ordering tensor characteristic equation. The orientational distribution function was calculated as a histogram of Euler beta angle $P(\beta)$ (the angle between the long axis of the molecule and director n). The higher values of angle fade for increased chirality of the nanotubes (Fig. 5.16).

The integral

$$N_{\Delta\beta}=\int_{\beta_1}^{\beta_2} P(\beta)\,d\beta \tag{5.2}$$

represents the number of molecules of the orientation between angles β_1 and β_2. In the range between 0° and 60° the number of molecules oriented within this range is $N = 25.3$ molecules for a (10, 10) and $N = 28.7$ molecules for a (18, 0) nanotube.

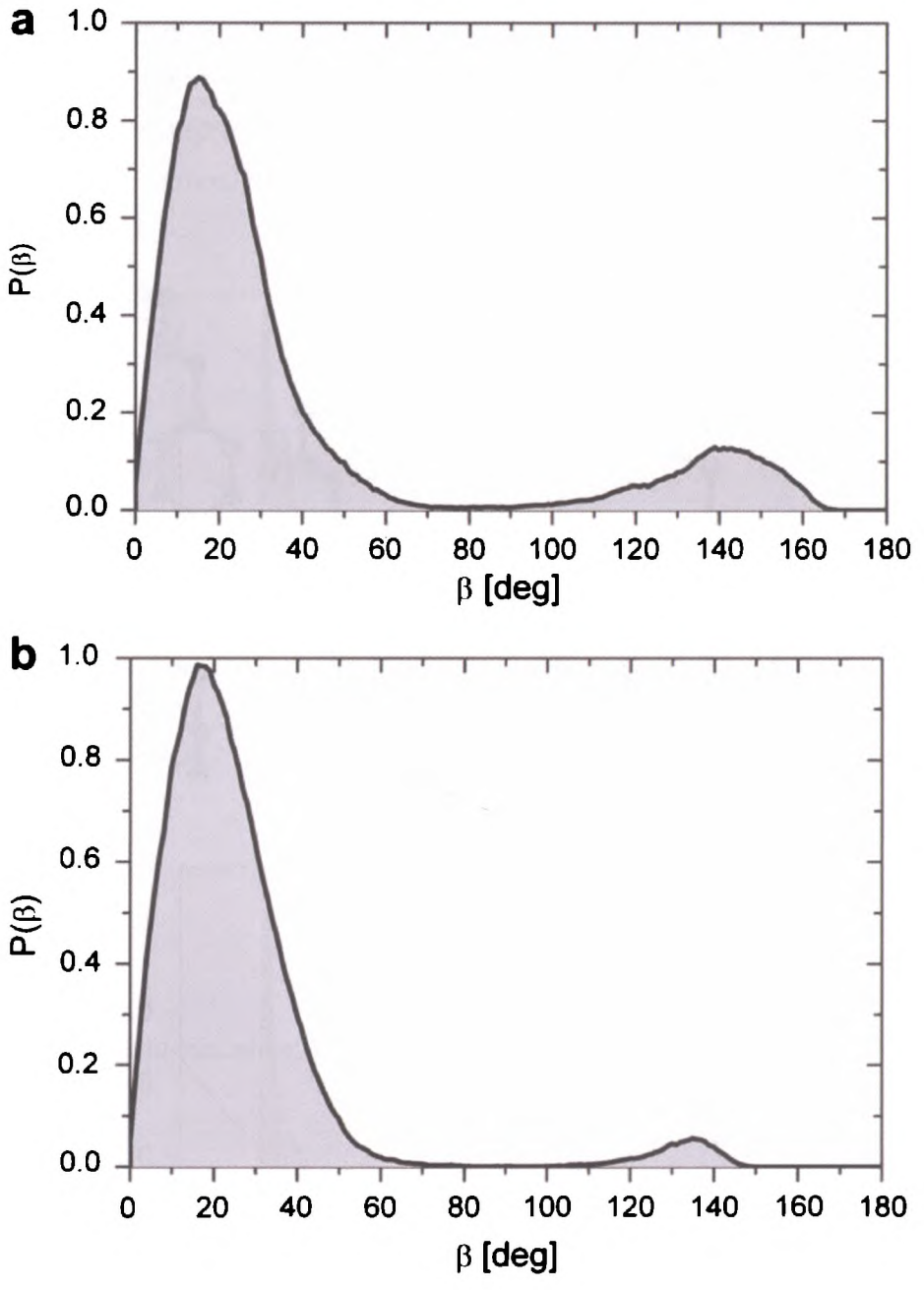

Fig. 5.16 Orientational distribution function $P(\beta)$ of chirality vectors a) (10, 10) and b) (18, 0) at $T = 300\ K$

The important fact is that zigzag SWCNT influences on the increasing of molecular order of liquid crystals located near such carbon surface.

My interest has been focused not only on the spatial order of mesogen molecules but on their dynamics as well. The translational movement of 5CB molecules has been investigated by the linear velocity autocorrelation function (Fig. 5.17).

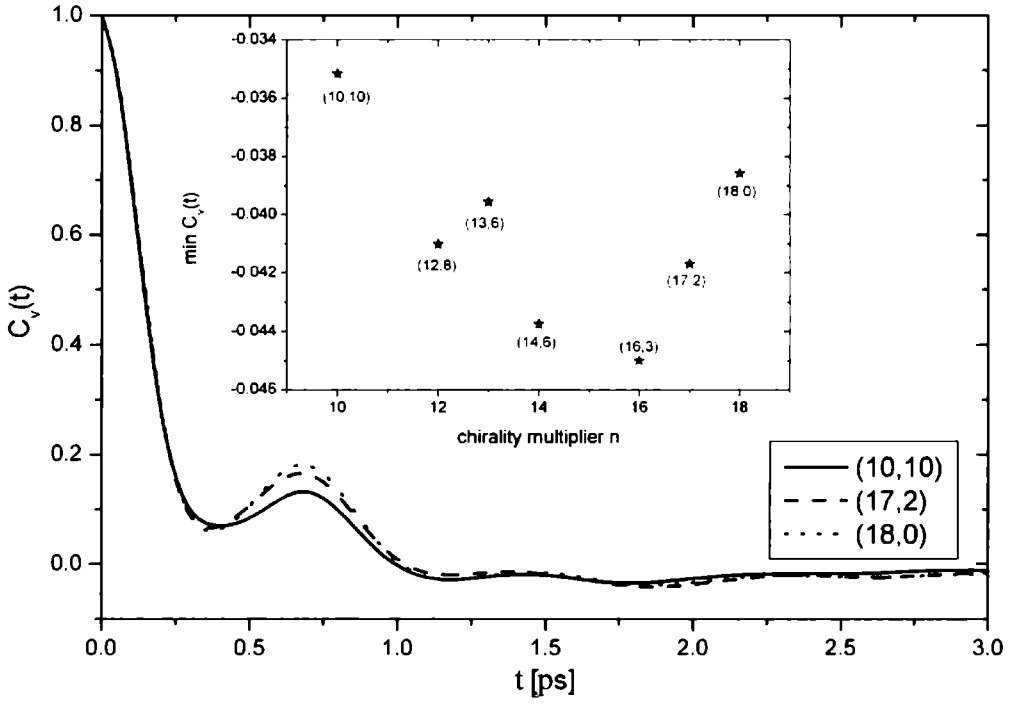

Fig. 5.17 Linear velocity of centre of mass autocorrelation function of 5CB molecules over three nanotubes of different chiralities at $T = 300\ K$

VACF goes to zero within 1.2 *ps*, in the chiral nanotubes $n \neq m \wedge n, m \neq 0$ the first dip depth is bigger than in armchair and zigzag nanotubes. This can be related to the jumps of the 5CB molecule over the hexagonal cell of a nanotube. The angular velocity autocorrelation function (AVCF) of liquid crystalline layer is presented in Fig. 5.18. The first dip depth in the AVCF changes with the chirality vector. For chiralities different than armchair and zigzag the depth of the first dip is smaller, see inset of Fig. 5.18. The plot suggests a very fast angular motion of mesogens, the function decays to zero within 0.6 *ps* [54].

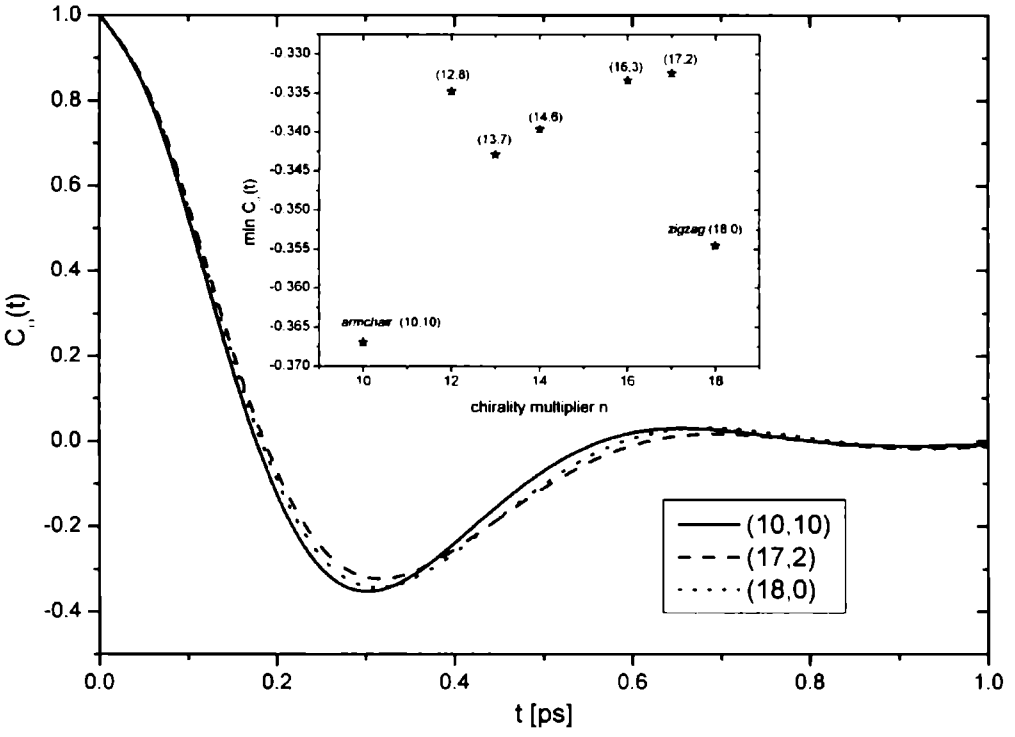

Fig. 5.18 Angular velocity autocorrelation function of 5CB molecules over three nanotubes of different chiralities at $T = 300\ K$

5.3 Mesogens confined in carbon nanotube

Molecular systems embedded in carbon nanotubes are interesting both from scientific point of view and also because of their interesting potential applications in energy storage, nanoelectronic devices, chemical biosensors, field emission displays and many others. Properties of molecules confined in carbon nanotubes have been intensively studied experimentally [55-57] and using computer simulation methods [58-62].

The simulated system consisted of forty 4-n-pentyl-4'-cyanobiphenyl (5CB) molecules encapsulated inside the single-walled, open-ended carbon nanotube. The diameter of SWCNT was chosen to be larger than mesogen length, to make enough space for rotational motions. 5CB molecule and SWCNT was modelled using flexible model based on CHARMM 27 force field. Interactions between the nanotube and 5CB mesogens have been described by L-J 12-6 potential with Lorentz-Berthelot mixing rules (details in section 4.1.1). Molecular structure and dynamics of 5CB molecules have been examined by calculating radial distribution functions, second rank order parameter and mean square displacement (parallel and

perpendicular to the director). The simulations were performed in NVT ensemble, for the room temperature (T = 300 K) and for T = 325 K. The temperature was controlled by Langevin thermostat with dumping coefficient $\gamma = 5.0\ ps^{-1}$.

The radial distribution function $g(r)$ of the mass centre of 5CB molecule is presented in Fig. 5.19. One can see that $g(r)$ distribution is characteristic for the cluster structure.

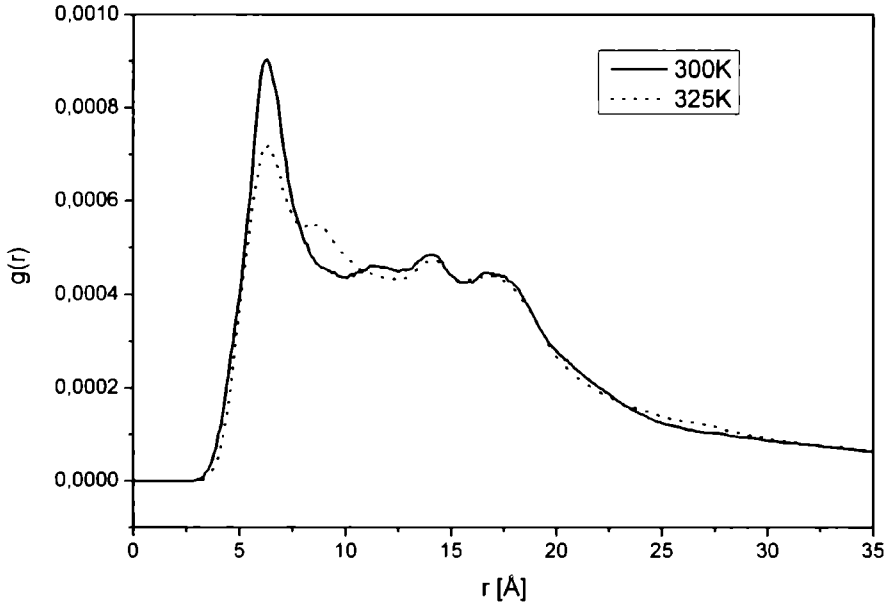

Fig. 5.19 The radial distribution function of 5CB inside SWCNT at T = 300 K and T = 325 K

The mean square displacement of a mass centre of 5CB molecules for two temperatures is presented in Fig. 5.20 The plots (Fig. 5.21 and Fig. 5.22) of the mean square displacement show a big difference between mesogens mobility parallel and perpendicular to the SWCNT surface (director has the same direction). The diffusion process along director occurs much faster than perpendicular diffusion and it is visible for both temperatures. It confirms strong anisotropic properties of 5CB material encapsulated by SWCNT. As one can see, the confinement of mesogens induces also higher molecular order in the cluster ($\langle P_2 \rangle$ = 0.77 at T = 300 K, $\langle P_2 \rangle$ = 0.76 at T = 325 K). The mobility of mesogens increases for the higher temperature but average order parameter doesn't go down. It is interesting and desired result. Both anisotropy and spatial order depend weak on the temperature so 5CB nematic phase might persist in a wide range of temperatures inside carbon nanotube.

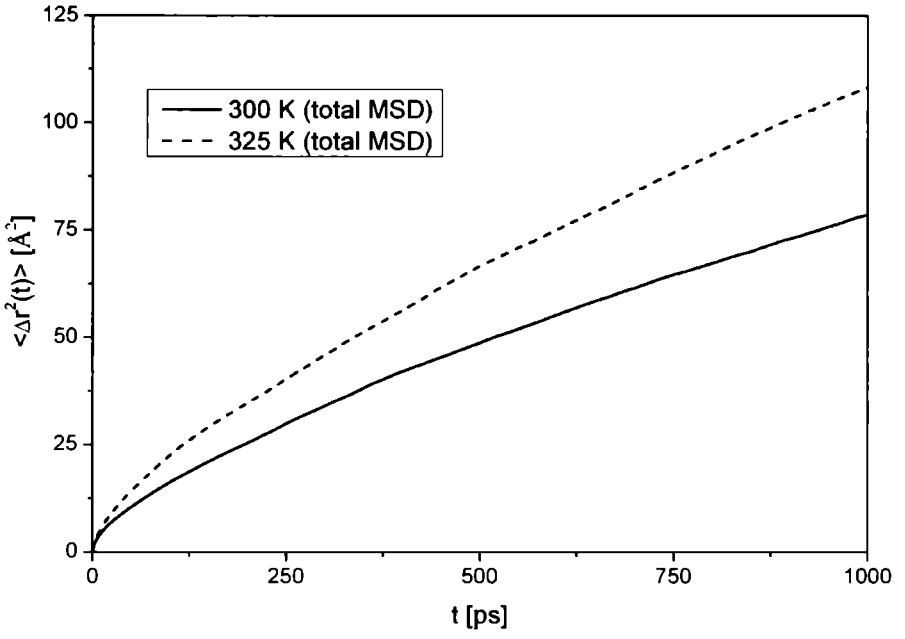

Fig. 5.20 The mean square displacement of the mass centre of 5CB molecule inside carbon nanotube, for two temperatures

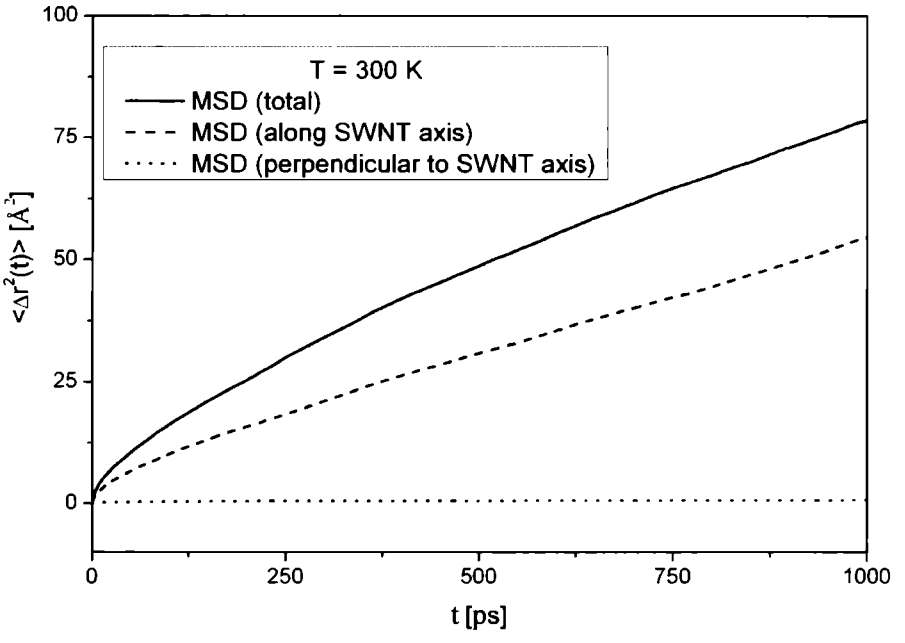

Fig. 5.21 The mean square displacement of the centre of mass of 5CB molecule inside carbon nanotube, calculated along different axes (directions)

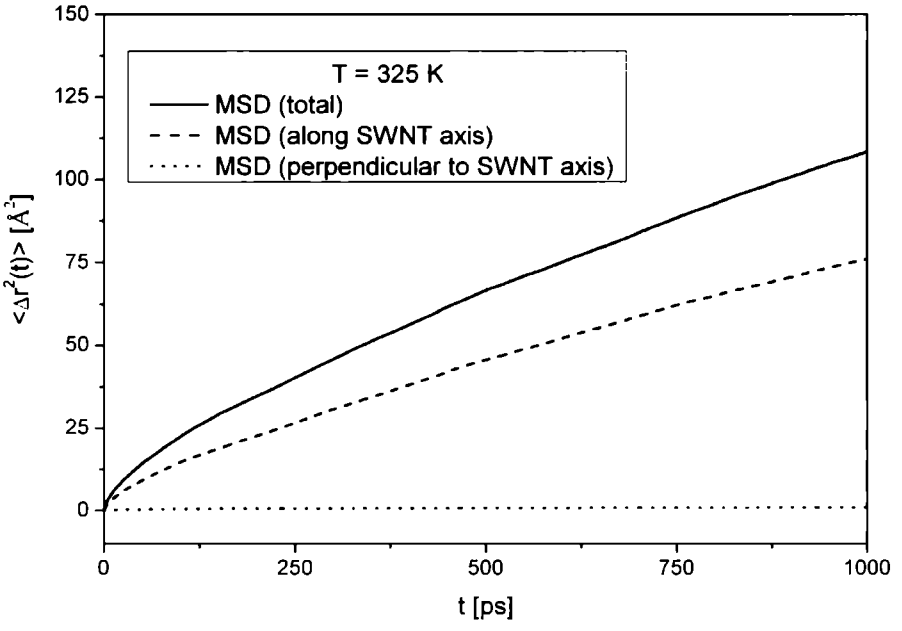

Fig. 5.22 The mean square displacement of the centre of mass of 5CB molecule inside carbon nanotube, at $T = 325\ K$ calculated along different axes (directions)

5.4 Liquid crystalline layer located between graphite walls

The dynamical properties of mesogens was also examined via MD study of the system consisted of 25 5CB molecules confined between two parallel graphite walls. The distance between graphite planes was adjusted in the range from 2.2 to 3.0 *nm*. The series of simulations were done at wide range of temperatures from $T = 100\ K$ to $T = 400\ K$.

Initially, liquid crystal molecules were aligned perpendicular to the graphite sheets forming a simple square 2D lattice. The molecular order in the layer has been checked by calculating the orientational distribution function as a histogram of angle between the long axis of a molecule and the eigenvector *n*. A broad distribution of orientation of 5CB molecules (long axis) can be observed at higher temperatures (see Fig. 5.23). Some molecules are oriented parallel to the graphite planes, which have been visualized instantaneous snapshot of MD simulation (Fig. 5.24).

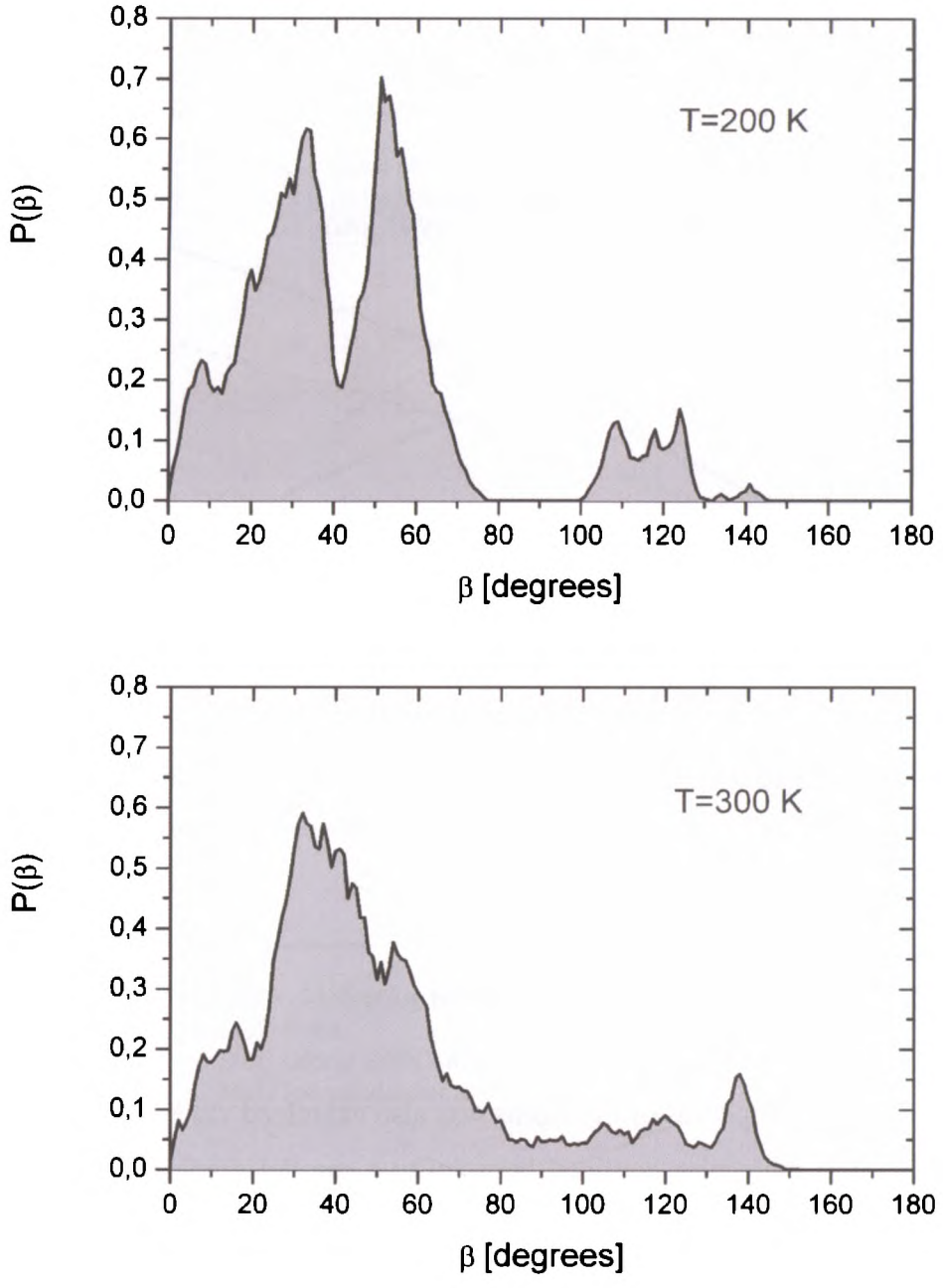

Fig. 5.23 The orientational distribution function of 5CB molecules at $T = 200\ K$ and at $T = 300\ K$

Dielectric properties analysis of 5CB cluster was done for range of temperatures and for different distances between graphite walls. The total dipole moment normalized autocorrelation function $C(t)$ is shown in Fig. 5.25. The higher the 5CB layer temperature, the faster is the dipolar relaxation because of a more vigorous motion of molecules.

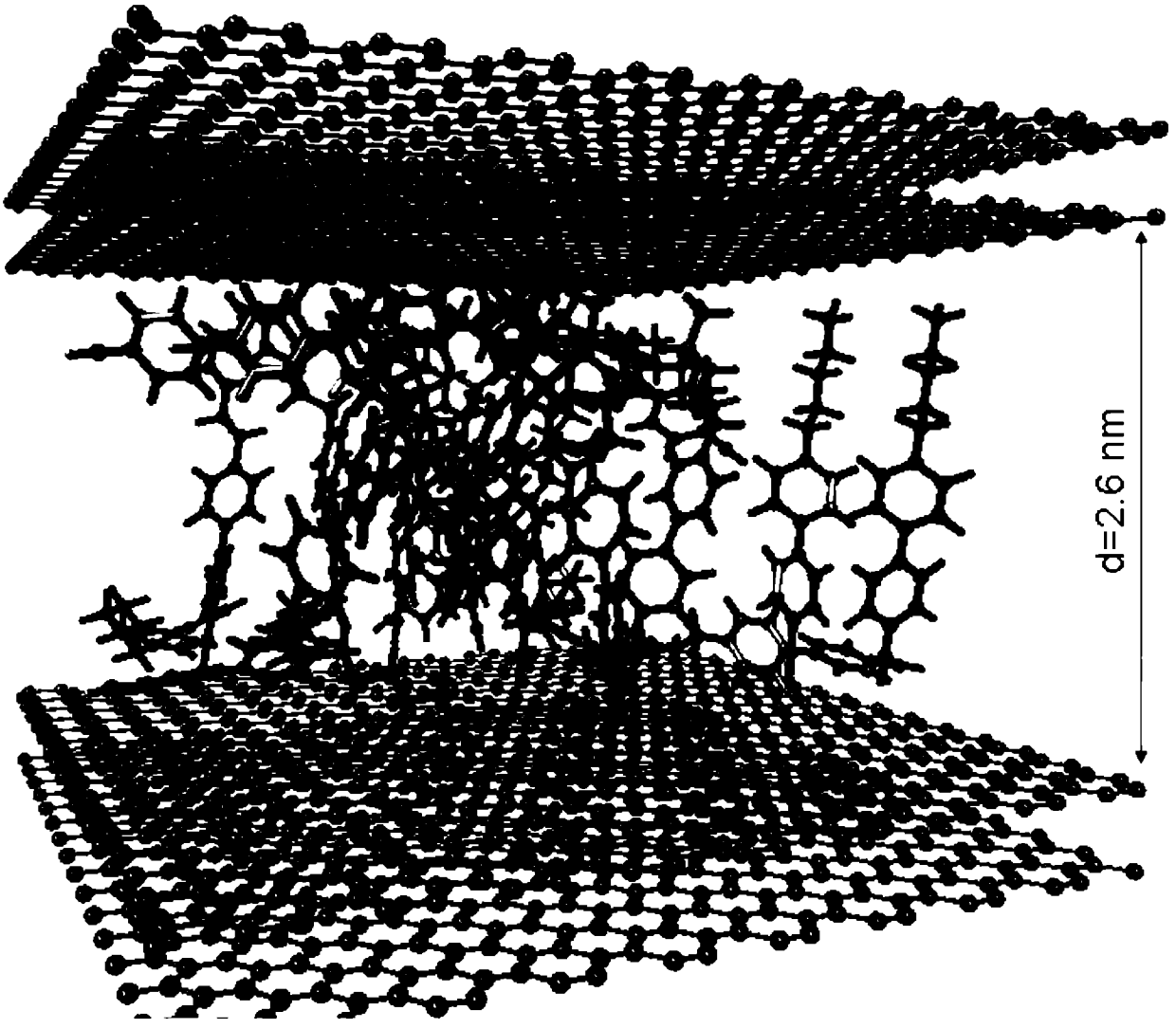

Fig. 5.24 A snapshot of 5CB molecules between graphite walls at $T = 300\ K$

The similar situation is also visible in the dielectric loss plot (Fig. 5.26). The maximum of dielectric loss $\varepsilon''(\omega)$ for $T = 100\ K$ is only 15% of the dielectric loss maximum at $T = 400\ K$. To obtain a low frequency part of $\varepsilon''(\omega)$, 10^{12} MD time steps would be required, compared to the $5 \cdot 10^6$ time steps that I had. The influence of variation of distance (from 2.2 to 3.0 *nm*) between the graphite planes was also investigated. The ensemble was equilibrated after each change of the separation distance and then the data were collected. When the planes are close to each other ($d = 2.2\ nm$) the function $C(t)$ decays very slowly (Fig. 5.27). Once the separation distance d increases (more space, more complicated dynamics) faster is the dipolar relaxation ($d = 3.0\ nm$).

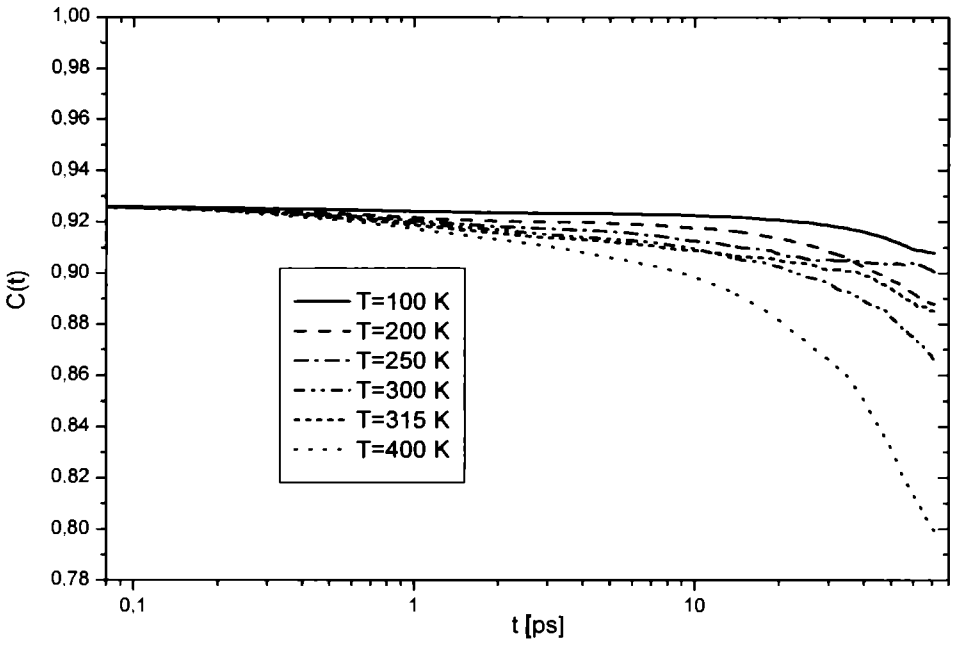

Fig. 5.25 The dipole moment autocorrelation function of 5CB (cluster between graphite walls) at several temperatures

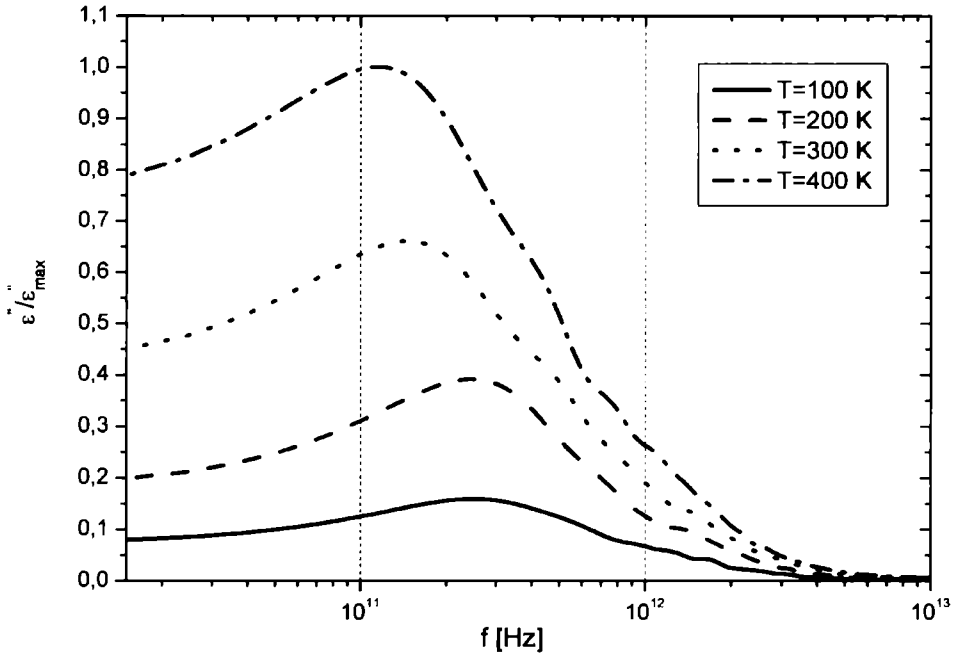

Fig. 5.26 The dielectric loss of 5CB cluster between graphite planes, normalized by the maximum loss at each temperature. Note that the frequency is in a log scale.

The maximum dielectric loss at $d = 2.4$ *nm* is 35% of the maximum dielectric loss for $d = 3.0$ *nm* (see Fig. 5.28). Moreover, the position of the maximum of $\varepsilon''(\omega)$ shifts towards lower frequencies when 5CB molecules have more space to rearrange their orientations.

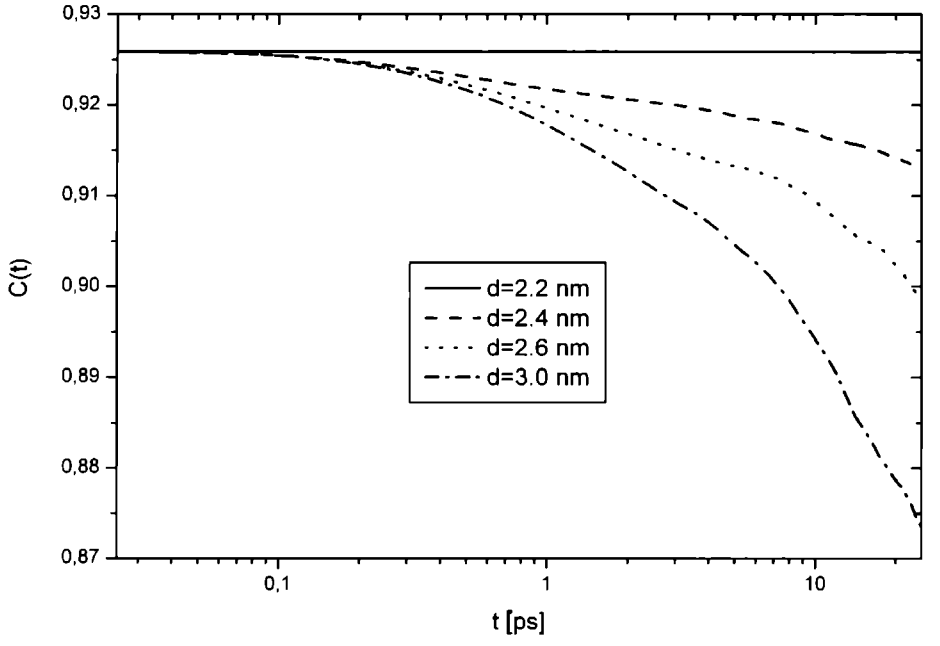

Fig. 5.27 The 5CB dipole moment autocorrelation function at several distancebetween graphite planes

Computer simulations of such specific physical ensemble show that the dynamics of mesogens depends not only on the temperature but also on the distance between the parallel graphite walls. The maximum dielectric loss lies between 120 – 260 *GHz* in the temperature range 100 *K* – 400 *K*.

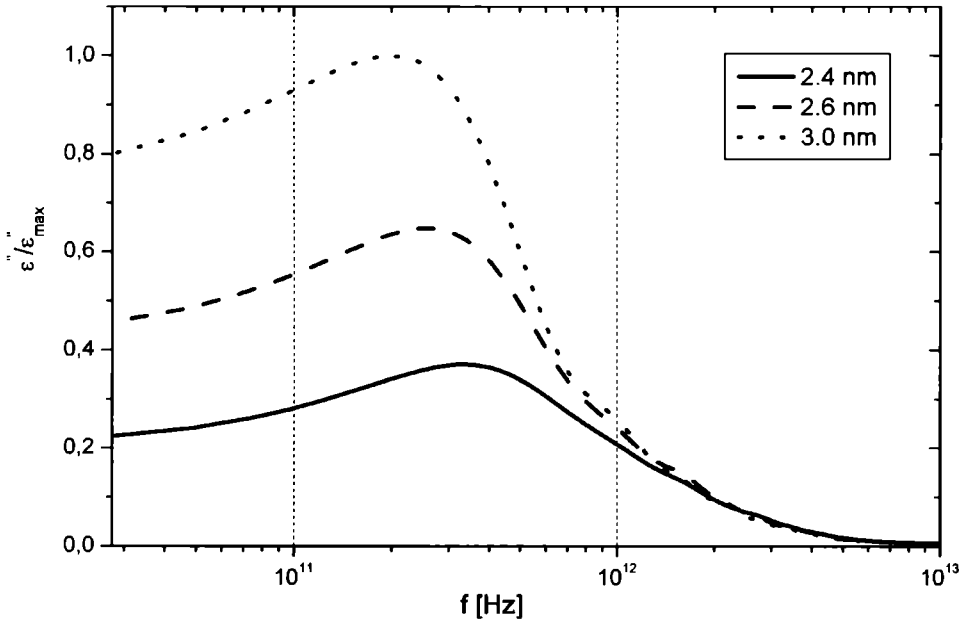

Fig. 5.28 The dielectric loss of 5CB cluster, normalized by the maximum loss at each distance between graphite planes at $T = 300$ *K*. Note that the frequency is in a log scale.

I also found the dielectric relaxation sensitivity of 5CB thin layer to a change of the separation distance d between the carbon surfaces. The position v_{max} of the maximum dielectric loss varies from 200 to 350 *GHz* for the room temperature. The physical foundation of the observed phenomena comes from the very complicated dynamics of liquid crystalline mesogens located near carbon structure. The given 5CB molecule is not only pushed and swirled by the neighbouring mesogens but also bounced (collides) with the carbon atoms of the graphite [63].

5.5 Mesogen molecules 5CB confined between graphene planes

In this section I consider the cluster of ninety eight 4-n-pentyl-4'-cyanobiphenyl molecules placed between two parallel graphene walls. I wanted to check if, and how, the peculiarities of the dynamics of molecules near graphene sheets influence the liquid crystalline properties (spatial ordering) of a small ensemble (cluster) mesogens confined between two parallel, one atom thick walls. Motivation to model and compute such physical ensemble in nanoscale is fact that some atoms and particles near graphene sheet have been already examined via different computer calculation techniques [64, 65] and experimentally studied [66].

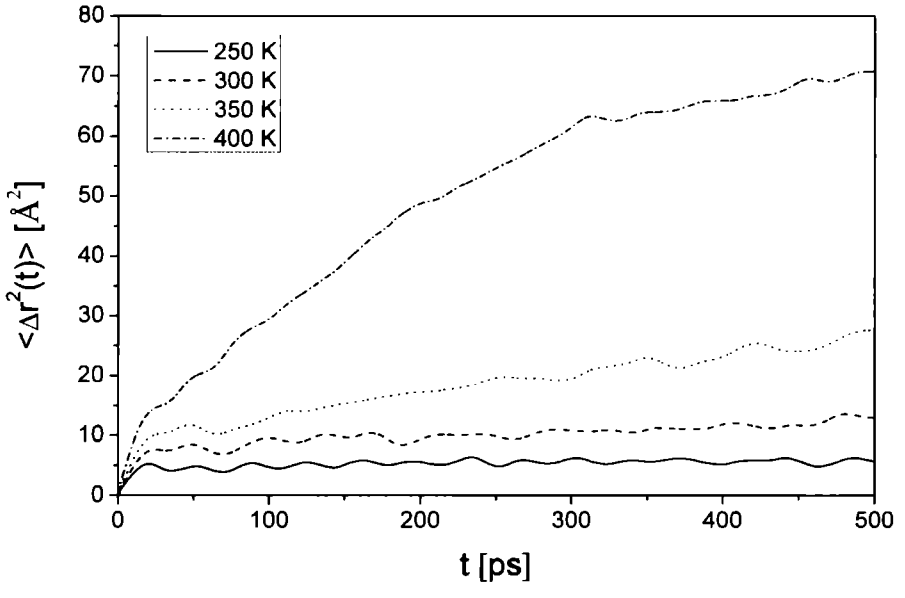

Fig. 5.29 The mean square displacement of the centre of mass of 5CB molecule at severaltemperatures

Physical properties of 5CB were calculated for several temperatures: the mean square displacement, translational and angular autocorrelation function, second rank order parameter. The separation distance between graphene planes was chosen $d = 44$ Å, it guarantees that 5CB molecules "feel" the influence of graphene surfaces but still have a space to perform the rotatory and translational motions. Each carbon sheet is built of 720 atoms and the area of graphene sheet was 44 Å · 44 Å = 1848 Å^2. The size of the simulated molecular cluster (consisted of 98 molecules) was matched to the restricted geometry of the system.

The course of the mean square displacement graph (Fig. 5.29) indicates that 5CB molecule can move only slightly within the cluster's volume for low temperatures. For example, the maximum displacement is around 2.2 Å at $T = 250$ *K* and 2.6 Å at $T = 300$ *K*. The plot of MSD reflects the efficient translational mobility of mesogen at the highest temperature studied.

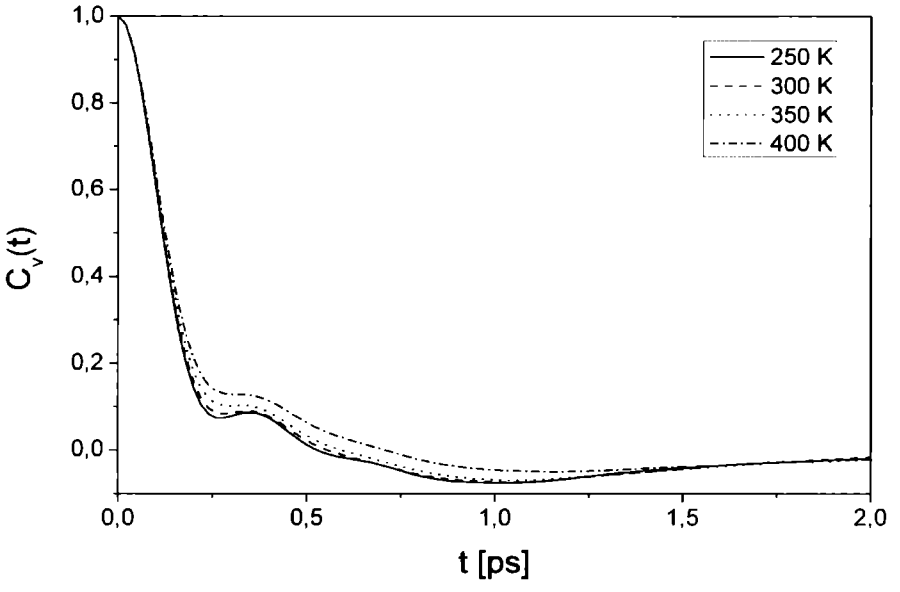

Fig. 5.30 The translational velocity autocorrelation function of 5CB molecule at several temperatures

To obtain further insight into mesogen molecules dynamics the normalized autocorrelation function $C_v(t)$ was calculated. Fig. 5.30 shows that – in spite of the huge mass of the 5CB molecule – its velocity changes rapidly, being almost entirely decorrelated after 1.5 *ps*. The temperature dependence of VACF is rather weak. Whereas the AVCF decays faster than $C_v(t)$ function what is visible in Fig. 5.31. The negative dip of $C_\omega(t)$ appears at $t \approx 0.25$ *ps*. The deep of negative dip changes with the temperature, the lower the temperature the greater is the dip of angular velocity autocorrelation function.

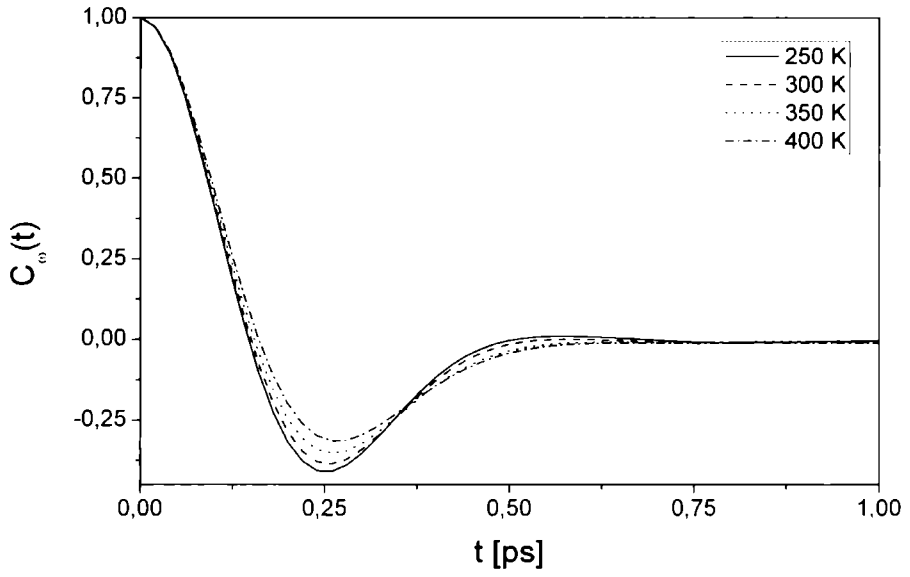

Fig. 5.31 The angular velocity autocorrelation function of 5CB molecule at several temperatures

A snapshot (see Fig. 5.32) from performed computer simulation of $(5CB)_{98}$ cluster at the room temperature reveals the evident spatial ordering (parallel to the graphene sheets) of $(5CB)_{98}$ cluster. The level of molecular order was tested via order parameter $\langle P_2 \rangle$ calculation.

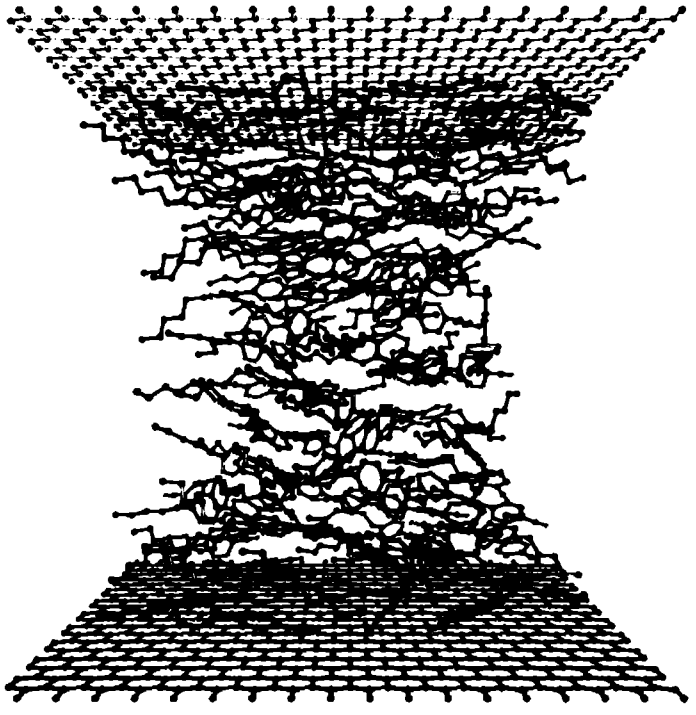

Fig. 5.32 The instantaneous configuration of $(5CB)_{98}$ system at $T = 300\ K$

Fig. 5.33 presents the temperature dependence of this observable. These high values of $<P_2>$ indicate liquid crystal ordering in the cluster which persists in quite remarkable temperature range 250 $K < T < 400$ K. What is also important the liquid crystal ordering in the cluster is quite stable in the presented "technical" temperature range. It only weakly declines with raising of the temperature. These properties of liquid crystal sample are essential when it comes to technological application. For comparison, the second rank order parameter for bulk 5CB sample (nematic phase) is $P_2^{bulk} \approx 0.64$ at $T = 300$ K [67]. The nematic–isotropic phase transition for bulk 5CB material appears at $T_{NI} = 308.5$ K [67] whereas liquid crystal nematic phase still exists in simulated mesogenic cluster embedded between graphene walls even at temperature as high as $T = 350$ K [68].

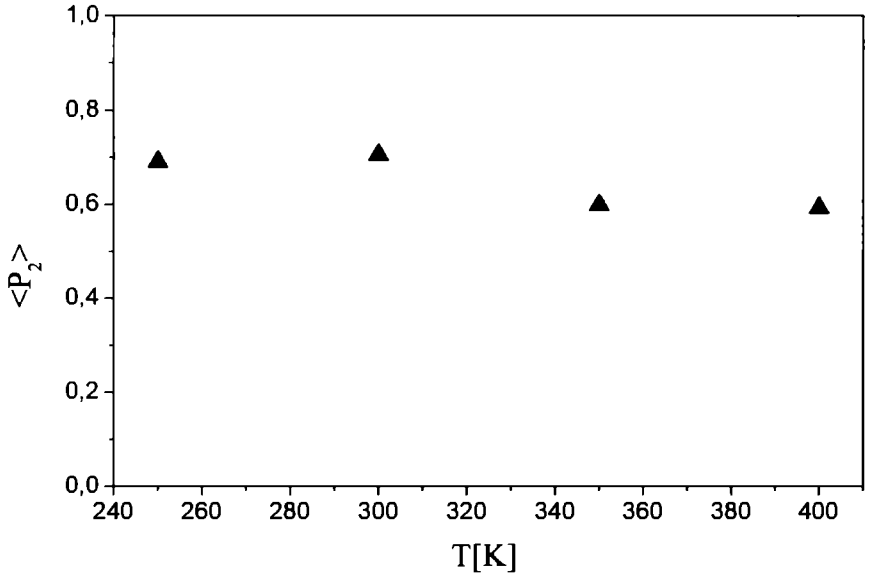

Fig. 5.33 The temperature dependence of the second rank order parameter (average value) of $(5CB)_{98}$ between graphene walls

5.6 Spatial order in different molecular systems

MD computer experiments have been done for many physical nanosystems (bulk 5CB sample, free cluster of 5CB, 5CB layer on SWCNT, thin layer of 5CB molecules near graphene plane, 5CB cluster confined in SWCNT, 5CB mesogens located between two graphene sheets). A large number of static and dynamic molecular characteristics of mesogens was presented in the previous sections of this dissertation. There is only one observable (order

parameter P_2), but really important for liquid crystals research, presented in this subsection. All calculations have been done and presented for the room temperature ($T = 300\ K$).

Table 5.2 Average value of second rank order parameter of 5CB mesogens at room temperature in different molecular systems

Ensemble ($T = 300\ K$)	Second rank order parameter $<P_2>$
5CB (bulk sample) – experimental data	0.64
5CB (bulk sample, boundary condition)	0.51
$5CB_{40}$ (free cluster)	0.35
$5CB_{40}$ (on SWCNT outer surface)	0.67
$5CB_{40}$ (inside SWCNT)	0.77
$5CB_{40}$ (on graphene plane)	0.65
$5CB_{40}$ (between 2 graphene sheets)	0.71

Table 5.2 contains data obtained from several different MD simulations and from real experiment. Computer experiment of 5CB bulk sample was performed in NPT ensemble for 196 molecules with periodic boundary conditions. Each other ensemble contains 40 liquid crystal molecules and simulations were performed in NVT ensemble without periodic boundary conditions.

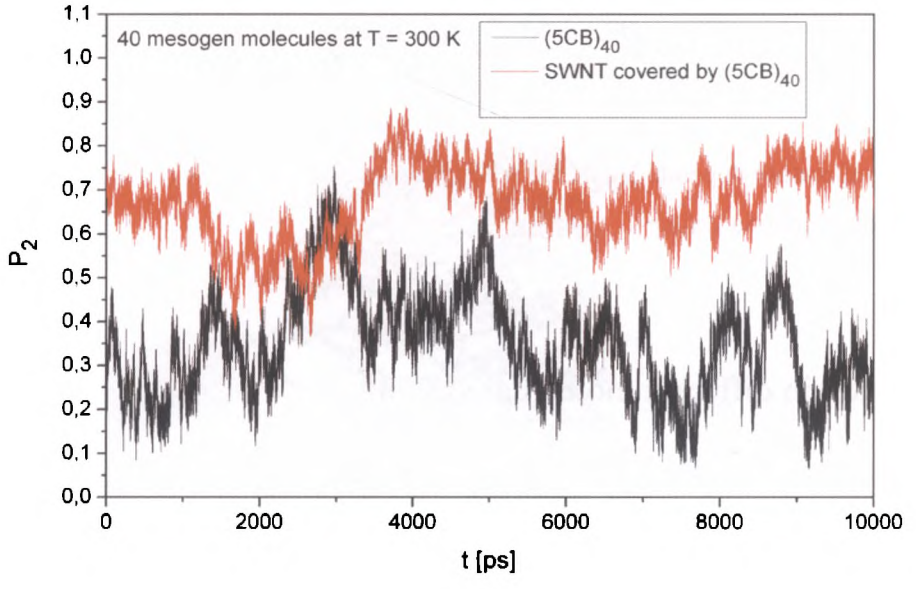

Fig. 5.34 Time evolution of P_2 for two different ensembles at $T = 300\ K$

5CB molecule and carbon structures were modelled using flexible model based on CHARMM 27 force field. As one can see Table 5.2 contains average values of second rank order parameter and time evolution of this quantity is shown in Fig. 5.34 for two chosen systems. It is easy to see that placing mesogens near carbon nanostructure (SWCNT, graphene) increases significantly spatial order of 5CB sample (60% - 100%). It is worth noting that the largest molecular order is visible in confined systems (5CB inside SWCNT, 5CB between 2 graphene planes). Let us also look at average value of $<P_2>$for bulk material. One can see that $P_2^{sim} < P_2^{exp}$ (20% less than experimental data). One of the reason of such difference might be fact that experimental sample contains much more molecules than computer modelled ensemble (196 · 5CB molecules). A typical slab of nematic for a twisted nematic display have around $2.4 \cdot 10^{11}$ molecules [69]. It should be emphasized that Proffesor Zannoni research group obtained very close result from MD simulation ($<P_2> \approx 0.51$ for $T = 300\ K$) [40].

SUMMARY

In my thesis I have focused on examining the structural and dynamic properties of $(5CB)_n$ clusters. Under normal circumstances, it appears that a bulk sample of 4-n-pentyl-4'-cyanobiphenyl changes dramatically its properties at the temperature about 310 *K*. Above this temperature pure 5CB sample occurs in isotropic phase and loses liquid crystalline properties. In this study I was able to show that placing 5CB molecules near the carbon nanostructures such as nanotube, graphite, or graphene increases the level of molecular order. Moreover, the second rank order parameter P_2 decreases slowly with an increasing of temperature. Therefore, the nematic phase of 5CB cluster may persist in wider temperature range, which is desirable in certain technical applications. Another important and interesting observation is that embedding 5CB mesogens inside SWCNT enhance the process of diffusion along director. The average value of the second rank order parameter is higher than in 5CB sample adsorbed on the outer surface of nanotube. Similar but weaker effect is observed in $(5CB)_n$ cluster confined between graphite or graphene sheets. It also appears that chirality of SWCNT has impact on the dynamics of liquid crystal layer located near carbon surface.

Some of the presented results seem to be of interest both from scientific point of view and also because of their potential applications in nanoelectronic devices, chemical biosensors and liquid crystal displays.

REFERENCES

1. P. G. de Gennes and J. Prost, The physics of liquid crystals, 2nd ed., Oxford University Press, (2003)
2. P. J. Collings, Liquid crystals: nature's delicate phase of matter, Princeton University Press, (1990)
3. Shri Singh, Liquid Crystals: Fundamentals, World Scientific Publishing Co. Pte. Ltd., (2001)
4. Michael R. Fisch, Liquid crystals, laptop and life, World Scientific Series in Contemporary Chemical Physics – vol. 23
5. S. Kumar, Liquid crystals in the nineties and beyond, World Scientific Publishing Co. Pte. Ltd., (1995)
6. D. Demus, J. Goodby, G. W. Gray, H.-W. Spiess, V. Vill,Physical properties of liquid crystals, Wiley-VCH, (1999)
7. Lev M. Bilnov, Structures and properties of liquid crystals, Springer, (2011)
8. C. Zannoni and M. Guerra, Molec. Phys., 44, 849, (1981)
9. F. Biscarini, C. Chiccoli, P. Pasini and C. Zannoni, Molec. Phys., 73, 439, (1991)
10. M. Abramowitz and I. A. Stegun, Handbook of Mathematical Functions. Dover Publications
11. V. Tsvetkov, Acta Physicoch. U.S.S.R., 10, 557, (1939)
12. G. R. Luckhurst and C. A. Veracini, The Molecular Dynamics of Liquid Crystals. Kluwer Academic Publisher
13. C. Zannoni, P. Pasini, Advances in the Computer Simulatons ot Liquid Crystals, Kluwer Academic Publishers, (2000)
14. R. Saito, G. Dresselhaus, M. S. Dresselhaus. Physical Properties of Carbon Nanotubes.
    Imperial College Press, (1998)
15. J. Singh, Physics of Semiconductors and their Heterostructures. New York,
    NY., McGraw-Hill, (1993)
16. S. Iijima, Nature (London) 354, 56, (1991)
17. S. Iijima, T. Ichihashi, Nature (London) 363, 603, (1993)
18. D. S. Bethune, C. H. Kiang, M. S. de Vries, G. Gorman, R. Savoy, J. Vazquez,

R. Beyers, Nature (London) 363, 605, (1993)
19. S. Reich, C. Thomsen, J. Maultzsch, Carbon nanotubes: Basic concepts and physical properties, Wiley-VCH, (2004)
20. M. S. Dresselhaus, G. Dresselhaus, Ph. Avouris, Carbon Nanotubes, Topics in Applied Physics, Springer, (2001)
21. M. S. Dresselhaus and Ph. Avouris, Introduction to Carbon Materials Research, Carbon Nanotubes, Topics Appl. Phys. 80, 1-9, (2001)
22. B. T. Kelly, Physics of graphite. London, Englewood, N.J., Applied Science, (1981)
23. R. H. Savage, Graphite Lubrication, Journal of Applied Physics 19(1): 1-10, (1948)
24. M. Dienwiebel, G. S. Verhoeven, et al., Superlubricity of Graphite, Physical Review Letters 92(12): 126101
25. Q. Zheng, B. Jiang, et al., Self-Retracting Motion of Graphite Microflakes, Physical Review Letters 100(6): 067205, 2008
26. P. R. Wallace, The Band Theory of Graphite, Physical Review 71(9): 622- 634, (1947)
27. K. S. Novoselov, A. K. Geim, S. V. Morozov, D. Jiang, Y. Zhang, S. V. Dubonos, I. V. Grigorieva, A. A. Firsov, Science 306 (2004) 666
28. D. Frenkel B. Smit, Understanding Molecular Simulation: From Algorithms to Applications, Academic Press, (2002)
29. N. Metropolis, A.W. Rosenbluth, M.N. Rosenbluth, A.H. Teller, and E. Teller, J. Chem. Phys. 21 (1953) 1087-1092
30. M. P. Allen, D. J. Tildesley, Computer Simulation of Liquids, Oxford University Press, (1989)
31. D. C. Rapaport, The Art of Molecular Dynamics Simulation, Cambridge University Press
32. D. Heermann, Computer simulation methods in theoretical physics, Second Edition, Springer-Verlag (1990)
33. An Introduction to Computational Physics Second Edition, Tao Pang, Cambridge University Press, (2006)
34. A. Hinchliffe, Molecular Modelling for Beginners, John Wiley and Sons, England, (2003)
35. A.V. Komolkin, A. Laaksonen, A. Maliniak, J. Chem. Phys. 101 (1994) 4103
36. W. Schmidt, K.K. Baldridge, J.A. Boatz, et al., J. Comput. Chem. 14205 (1993) 1347.
37. L.G. MacDowell y C. Vega, J.Chem.Phys. 109, 5681 (1998)
38. H. Fukunaga, J. Takimoto, M. Doi, J. Chem. Phys. 120, 7792 (2004)

39. M. R. Wilson, Chem Soc Rev., (2007), 36 (12), 1881-8

40. Tiberio G., Muccioli L., Berardi R., Zannoni C., Chemphyschem (2009) Jan 12; 10(1):125-36

41. A.D. MacKerell Jr, M. Feig, C.L. Brooks III, J. Comp. Chem. 25 (2004) 1400; 316 S. Feller, A.D. MacKerell Jr, J. Phys. Chem. B 104 (2000) 7510

42. E. Guàrdia, J. Martí, Phys. Rev. E 69 (2004) 011502

43. A.K. Jonscher, Dielectric Relaxation in Solids, Chelsea Dielectric Press, London, 308 (1983)

44. Molecular-Dynamics Simulation of Statistical-Mechanical Systems, G. Ciccotti and W. G. Hoover (1986)

45. M. E. Rose, Elementary Theory of Angular Momentum, Wiley, NewY ork, (1957)

46. C. Zannoni, in The Molecular Physics of Liquid Crystals, (eds. G. R. Luckhurst, G. W. Gray), Academic Press, London, (1979) pp. 191–220

47. R. Eppenga, D. Frenkel, Mol. Phys. (1984), 52, 1303–1334

48. A. Brunger, C.L. Brooks, M. Karplus, Chem. Phys. Lett. 105 (1984) 495

49. J.C. Phillips, R. Braun, W. Wang, J. Gumbart, E. Tajkhorshid, E. Villa, C. Chipot, R.D. 314 Skeel, L. Kale, K. Schulten, J. Comput. Chem. 26 (2005) 1781

50. W. Gwizdała, A. Dawid and Z. Gburski, Solid State Phenomena Vol. 140 (2008) pp 89-96

51. G. Stan et al., Phys. Rev. B 62 (2000) 2173

52. W. Gwizdała, K. Górny, Z. Gburski, Journal of Molecular Structure 887 (2008) 148-151

53. H. Rafii-Tabar; Computational Physics of Carbon Nanotubes, Cambridge University, Cambridge, (2008)

54. A. Dawid, W. Gwizdała, Journal of Non-Crystalline Solids 355 (2009) 1302-1306

55. A.I. Kolesnikov, J.M. Zanotti, C.K. Loong, P. Thiyagarajan, A.P. Moravsky, R.O. 289 Loutfy, C.J. Burnham, Phys. Rev. Lett. 93 (2004) 35503

56. M.P. Rossi, H. Ye, Y. Gogotsi, S. Babu, P. Ndungu, J.C. Bradley, Nano Lett. 4 (2004) 291 989

57. B.M. Kim, S. Sinha, H.H. Bau, Nano Lett. 4 (2004) 2203

58. Z. Dendzik, K. Górny, Z. Gburski, J. Phys. Condens. Matter 21 (2009) 425101

59. J. Marti, M.C. Gordillo, J. Chem. Phys. 114 (2002) 10486

60. G. Garberoglio, Eur. Phys. J. E 31 (2010) 73

61. Y. Lin, J. Shiomi, S. Maruyama, G. Amberg, Phys. Rev. B 80 (2009) 045419
62. J. Kofinger, C. Dellago, Phys. Rev. Lett. 103 (2009) 080601
63. A. Dawid and W. Gwizdała, Rev.Adv.Mater.Sci 23 (2010) 37-41
64. O. Leenaerts, B. Partoens, F. M. Peters, Microelectronics Journal 40 (2009) 860-862
65. R. Varns and P. Strange, J. Phys: Condens. Matter 20 (2008) 225005 (8pp)
66. A. Hashimoto, H. Terasaki, A. Yamamoto, S. Tanaka, Diamond & Related Materials 18 (2009) 388-391
67. I. Vecchi, A. Arcioni, C. Bacchiocchi, G. Tiberio, P. Zanirato, C. Zannoni, Mol. Cryst. Liq. Cryst., 465 (2007) 271
68. W. Gwizdała, K. Górny, Z. Gburski, Spectrochimica acta. Part A, Molecular and biomolecular spectroscopy, 79 (4), p.701-704, (2011)
69. M. R. Wilson, Int. Rev. Phys. Chem., (2005), 24, 421-455